The NF45/NF90 heterodimer contributes to the biogenesis of 60S ribosomal subunits and influences nucleolar morphology

Franziska Wandrey,[a] Christian Montellese,[a,b] Krisztián Koós,[c] Lukas Badertscher,[a,b] Lukas Bammert,[a,b] Atlanta G. Cook,[d] Ivo Zemp,[a] Peter Horvath,[c] and Ulrike Kutay,[a,#]

[a] Institute of Biochemistry, ETH Zurich, Zurich, Switzerland
[b] Molecular Life Sciences Ph.D. Program, Zurich, Switzerland
[c] Synthetic and Systems Biology Unit, Hungarian Academia of Sciences, BRC, Szeged, Hungary
[d] Wellcome Trust Centre for Cell Biology, University of Edinburgh, Max Born Edinburgh, EH93BF, U.K.

Running Head: NF45 and NF90 contribute to human ribosome biogenesis

[#]Address correspondence to Ulrike Kutay, ulrike.kutay@bc.biol.ethz.ch

Keywords: NF45, NF90, ILF2, ILF3, 60S, ribosome biogenesis, nucleolus

Abbreviations: dsRBD, double-stranded RNA binding domain; DZF, domain associated with zinc fingers; HASt-tag, hemagglutinin-epitope/streptavidin-binding peptide tag; LMB, leptomycin B; NLS, nuclear localization signal; rRNA, ribosomal RNA; StHA-tag, streptavidin-binding peptide/ hemagglutinin-epitope tag; TAP, tandem affinity purification

Word count of abstract: 198
Word count of main text: ~ 37'100

ABSTRACT

The interleukin enhancer binding factors ILF2 (NF45) and ILF3 (NF90/NF110) have been implicated in various cellular pathways such as transcription, miRNA processing, DNA repair and translation in mammalian cells. Using tandem affinity purification, we identified human NF45 and NF90 as components of precursors to 60S ribosomal (pre-60S) subunits. NF45 and NF90 are enriched in nucleoli and co-sediment with pre-60S particles in density gradient analysis. We show that association of the NF45/NF90 heterodimer with pre-60S particles requires the double-stranded RNA binding domains of NF90 while depletion of NF45 and NF90 by RNA interference leads to a defect in 60S biogenesis. Nucleoli of cells depleted for NF45 and NF90 have an altered morphology and display a characteristic spherical shape. These effects are not due to impaired rRNA transcription or processing of the precursors to 28S ribosomal RNA (rRNA). Consistent with a role of the NF45/NF90 heterodimer in nucleolar steps of 60S subunit biogenesis, downregulation of NF45 and NF90 leads to a p53 response accompanied by induction of the cyclin-dependent kinase inhibitor p21/CIP1, which can be counteracted by depletion of RPL11. Together, these data indicate that NF45 and NF90 are novel, higher eukaryote-specific factors required for the maturation of 60S ribosomal subunits.

INTRODUCTION

The nuclear factors NF45 and NF90 (NFAR-1, DRBP76, MPP4, TCP80) were originally discovered as a heterodimeric complex binding to the interleukin-2 (IL-2) promoter (1, 2), and are also referred to as interleukin enhancer-binding factors 2 (ILF2) and 3 (ILF3), respectively (3). While NF90 is vertebrate-specific, NF45 is found throughout metazoans.

In mammals, the NF45/NF90 complex is widely expressed across tissues (4). Over the recent years, NF45/90 has been implicated in a great variety of biological processes. Apart from regulation of transcription (5-7), the heterodimer has also been linked to numerous other pathways such as DNA damage response (8, 9), mRNA metabolism (10, 11), miRNA biogenesis (12), and viral infection (13-17). NF90 knockout mice display severe defects in skeletal muscle formation leading to respiratory failure soon after birth (18), indicating an essential role of NF90 function in vertebrate development.

Both NF45 and NF90 possess an N-terminal ‘domain associated with zinc fingers’ (DZF) that is only found in metazoan proteins. Recent structural analysis revealed that the DZF domains of NF45 and NF90 resemble template-free nucleotidyltransferases and mediate their heterodimerization through a structurally conserved interface (19). In addition to the DZF domain, NF90 possesses two double-stranded RNA binding domains (dsRBDs) in the C-terminal region (2, 20) that confer binding to highly structured RNAs (21-23).

NF90 is expressed from at least five alternatively spliced mRNAs that all encode for the DZF and dsRBDs. Some of the splice variants generate C-terminally extended protein isoforms referred to as NF110 (NFAR-2) (24, 25), which also interact with NF45 (26). Compared to NF90, NF110 displays a stronger association with chromatin, and has been mainly linked to transcription (26-28).

Interestingly, NF45 and NF90 have been identified as part of the nucleolar proteome by mass spectrometric analysis (29, 30). The biological significance of this potential nucleolar localization has, however, not been explored. The main function of nucleoli is ribosome synthesis and the majority of characterized nucleolar factors support this task. Nucleolar steps of ribosome

biogenesis comprise synthesis of ribosomal RNA (rRNA) precursors, rRNA folding, processing and modification, as well as the assembly of the majority of ribosomal proteins. A plethora of factors, called trans-acting factors, associate with pre-ribosomal particles at different time points in their maturation pathway. Most of these trans-acting factors have been originally identified by proteomic analysis of pre-ribosomal particles (reviewed in (31-35)).

Here we show that the NF45/NF90 heterodimer is a novel component of human pre-60S ribosomal particles. Whereas the dsRBDs of NF90 are required for association with pre-60S, binding to NF45 is dispensable for pre-60S binding. Depletion of NF45 or NF90 leads to defects in ribosome biogenesis as well as to a change in nucleolar architecture, indicating an early role of the NF45/NF90 dimer in 60S biogenesis.

MATERIALS AND METHODS

Cell lines, antibodies and reagents

The RPL29-GFP and RPS2-YFP reporter HeLa cell lines, and the ZNF622-StHA, MRTO4-StHA, HASt-PNO1, HASt-LTV1, HASt-GFP-expressing HEK293 FlpIn TRex cell lines have been described previously (36, 37). The RPL26-GFP HeLa cell line was generated by integrating RPL26-GFP into HeLa K FRT TetR cells as described for RPL29-GFP (36). Polyclonal HEK293 FlpIn TRex cell lines for NF90-TAPs and the NF90-expressing HeLa FlpIn cell line for rescue experiments were generated as previously described (37, 38).
Anti-NF45 (sc-365283), anti-ILF3 (sc-136197), anti-ZNF622 (sc-100980), anti-FBL (sc-166001), anti-MRTO4 (sc-81856), anti-UBF (sc-13125), anti-eIF6 (sc-390441), and anti-p21 (sc-756) were purchased from Santa Cruz Biotechnologies, anti-NF110 (EPR3627) from GeneTex, anti-NPM (B0556), anti-α-tubulin (T5168) and anti-GAPDH (G8795) from Sigma Aldrich, anti-HNRNPC (ab10294) and anti-RPL5 (ab86863) from Abcam, anti-p53 (554293) from Becton Dickinson and anti-HA (MMS-101P) from Covance. The following antibodies have been previously described: anti-RPS3, anti-RIOK2, anti-NMD3 (39), anti-NOC4L (37), anti-RPL23 (40), anti-XPO5, anti-CRM1 (41), anti-RLP24 (36) and anti-LSG1 (40). Secondary antibodies for immunofluorescence were purchased from Invitrogen (LuBioScience, Switzerland). LMB (L-6100) was purchased from LC Laboratories.

Molecular cloning

A cDNA clone comprising the NF90 coding sequence was ordered from SourceBioScience. The NF90 ORF was subcloned in full length or C-terminal truncations into the pcDNA5/FRT/TO/nHASt-TAP vector (37) using BamHI/NotI. NF110 was obtained by amplification of a fragment of the DNA sequence common to NF90 and NF110 and ligation by Gibson assembly to a synthetic DNA fragment encoding the NF110-specific sequence. The NF110 sequence was then cloned into the pcDNA5/FRT/TO/nHASt-TAP vector using KpnI/NotI. NF90 point mutations were introduced using the QuikChange kit (Agilent Technologies). An siRNA-resistant construct of HASt-NF90 was

generated by replacing part of the NF90 coding sequence by a synthetic DNA fragment (GeneArt, Invitrogen) of the same region containing silent mutations at the binding site of the si-NF90/110 siRNA using the internal restriction sites PstI/HindIII. The coding region of RPL26 was amplified from HeLa cell cDNA and cloned into the KpnI/BamHI sites of pcDNA5/FRT/TO/GFP.

Cell fractionation

HeLa cells were detached with PBS containing 0.5 mM EDTA and washed in 10 mM Tris/HCl (pH 7.5), 10 mM KCl and 2 mM $MgCl_2$. Lysis was performed by passage through a 27G needle in ice-cold buffer containing 10 mM Tris/HCl (pH 7.5), 10 mM KCl, 2 mM $MgCl_2$, 1 mM EGTA, 1mM DTT, and protease inhibitors. After lysis, cells were centrifuged at 2000 x g for 5 min at 4°C. The supernatant was used as cytoplasmic extract and the pellet containing the cell nuclei was washed twice with lysis buffer before a sample was taken for Western blot analysis.

RNAi, transient transfections

Transient transfection of DNA into cells was performed using X-tremeGENE 9 DNA Transfection Reagent (Roche) and cells were fixed after 24 h using 4% PFA.

Transfection of siRNAs into HeLa K and U2OS cells was carried out using INTERFERin transfection reagent (Polyplus transfection). For HeLa FlpIn and HEK293 FlpIn TRex cells, Lipofectamine RNAiMAX Reagent (Invitrogen) was used. The siRNA oligonucleotides were used at 9 nM concentration, except for si-RPL11, si-RPL23 and si-PES1, which were used at 4.5 nM concentration. The following siRNA oligos were used in this study:

AllStars siRNA (Qiagen) served as negative control (si-control); si-NF45 (5'-CUCCAUAGAAGUGUCAUUCCA-3'); si-NF90/110 (5'-GUGGAGGUUGAUGGCAAUUCA-3'); si-NF90/110-2 (5'-CACAACCGCCCUCCUGGACAA-3'); si-POLR1A (5'-AAGGAUGUAGUUCUGAUUCGA-3');
si-RPL11 (5'- GGUGCGGGAGUAUGAGUUA-3'); si-PES1 (5'-CCGGCUCACUGUGGAGUUCAU-3'); si-RPL23 (5'-GUGGUCAUUCGACAACGAU-3'); si-XPO5 (5'-

AGAUGCUCUGUCUCGAAUU-3'); si-ZNF622 (5'-CAGGCACAUAUGAAUGACAAA-3'); si-AAMP (5'-CTGGACTTTGCCCTCAGCAAA-3').

Tandem affinity purification and MS analysis

Cell extract preparation and TAP as well as subsequent mass-spectrometry analysis of eluted proteins was carried out as described in (37).

Sucrose gradient analysis

For the sucrose gradient analysis depicted in Fig. 1C, HeLa K cells were treated with 100 µg/ml cycloheximide and lysed in 50 mM HEPES/KOH pH 7.5, 100 mM KCl, 3 mM $MgCl_2$, 0.5% NP-40, 1 mM DTT, 100 µg/ml cycloheximide, and protease inhibitors. The lysate was centrifuged (16,000 x g for 5 min at 4°C) and the supernatant was used for gradient analysis. For the sucrose gradients analysis depicted in Fig. 6C, HeLa K cells were treated with 100 µg/ml cycloheximide and lysed in 10 mM Tris/HCl pH 7.4, 100 mM KCl, 10 mM $MgCl_2$, 1% Triton X-100, 1 mM DTT, 100 µg/ml cycloheximide, and protease inhibitors. The lysate was incubated on ice for 5 min, centrifuged (10'000 g for 3 min at 4°C) and the supernatant was used for gradient analysis. Extracts (400 µg of total protein) were loaded onto a linear 10%-45% sucrose gradient in 50 mM HEPES/KOH pH 7.5, 100 mM KCl, 3 mM $MgCl_2$. After centrifugation for 105 min at 55,000 rpm at 4°C in a TLS55 rotor (Beckman Coulter), 150 µl fractions were precipitated with TCA and used for Western blotting.

Immunofluorescence (IF)

Cells were fixed with 4% PFA for 15 min and permeabilized in 0.1% Triton and 0.02% SDS in PBS for 5 min. For anti-ILF3 IF, cells were permeabilized in acetone (5 min, -20°C). For anti-NF45 IF, cells were fixed/permeabilized in 1:1 methanol/acetone (10 min, -20°C). IF was carried out as previously described (39).

Confocal microscopy

Pictures of cells were taken with a Leica SP1 TCS confocal microscope or a Leica SP2 AOBS confocal scanning system with a 63x objective.

Northern Blotting

RNA was extracted from HeLa K cells using the RNeasy mini kit (Qiagen). 3 µg RNA per lane was separated on an agarose gel (1.2% agarose in 50 mM HEPES pH 7.8, 6% formaldehyde). The RNA was stained by incubating the gel for 1 h in 3x GelRed solution (Biotium) and transferred to a Nylon membrane (Hybond, GE Healthcare) by capillary transfer. The RNA was cross-linked to the membrane via UV-crosslinking (Stratalinker, Fisher Scientific). The membrane was stained with GelRed to control for uniform transfer. After pre-hybridization of the membrane for 1 h in 50% formamide, 5x SSPE, 5x Denhardt's solution, 1% SDS, 200 µg/ml DNA from fish sperm (Roche) at 65°C, a radiolabeled probe (either 5'ITS1 (5′-CCTCGCCCTCCGGGCTCCGTTAATGATC-3′) or ITS2 (5′-GCGCGACGGCGGACGACACCGCGGCGTC-3′) previously described in (42)) was added to the buffer and, after further incubation at 65°C for 1 h, the membrane was hybridized at 37°C overnight. The membrane was washed twice with 2x SSC for 5 min at 25°C and analyzed by phosphoimaging.

Nucleolar quantification program

A Matlab-based (Sunnyvale, CA, USA) image processing software was written to segment cells and their nucleoli and analyze morphological and intensity-based properties. A graphical user interface was developed allowing interactive semi-manual analysis and data browsing. Multiple fluorescent images can be loaded, consisting each of up to 3 spectral channels. The first channel containing the DNA staining was used to identify individual nuclei, while the second channel was used to detect nucleoli based on immunofluorescence of eIF6. Images were segmented using the Otsu thresholding algorithm (43). A nucleolus was considered to belong to a nucleus if its segmented area was inside the nuclear area. Objects not segmented properly were excluded manually by the user. After the selection process, a CSV statistics file containing the intensity and morphological

parameters of all the selected nucleoli was generated and used for statistical analysis.

XPO5 binding assay

MRTO4-StHA HEK 293 FlpIn TRex cells were either left untreated or treated with siRNAs against NF45 (9 nM) and NF90/NF110 (18 nM) for 72 h and harvested as described above. TAP followed by an exportin binding assay was performed as previously described (36).

Double-thymidine block

HeLa K cells were treated with 3 mM thymidine (Sigma Aldrich) for 15 h and released by washing with Dulbecco's Modified Eagle's Medium (Sigma Aldrich). Cells were incubated in medium for 9 h and treated again with 3 mM Thymidine for 16 h before harvesting.

Cell staining and cell cycle analysis

HeLa K cells were detached with PBS containing 0.5 mM EDTA and washed in PBS. Cells were fixed by the addition of 70% ethanol while vortexing and stored at -20°C. To stain the DNA, cells were centrifuged (300 g, 5 min) and stained with buffer (1 mg/ml sodium citrate, 0.3% v/v Triton X-100, 20 µg/ml RNase A) containing 100 µg/ml propidium iodide (Sigma Aldrich) before analysis. Cells were analyzed at the ETHZ Flow Cytometry Facility using a BD LRS Fortessa with excitation wavelengths of 561 nm or 405 nm and the emission was detected at 610/620 nm. Data was analyzed with FlowJo (Version 9.6.7) using the Watson (Pragmatic) and the Dean-Jett-Fox models.

Fluorescence in situ hybridization (FISH)

Fluorescence in situ hybridization analysis was performed as previously described (42) using a 5'ETS-specific probe (5'-Cy5-GCACCGGGAGTCGGGACGCTCGGACGCGCGAGAGAACAGCA-3'; previously described in (44)).

RESULTS

NF45 and NF90 are associated with pre-60S particles

To investigate the composition of human pre-60S ribosomal particles, we performed tandem affinity purification (TAP) using ZNF622 tagged with a C-terminal tandem streptavidin-binding peptide (St) and hemagglutinin epitope (HA) tag expressed in HEK293 cells as bait (Figure 1). ZNF622 is the human homolog of the *S. cerevisiae* 60S subunit trans-acting factor Rei1 (45, 46), and has been previously shown to associate with pre-60S subunits in HeLa cells (36). As expected, mass spectrometric analysis of proteins co-purifying with ZNF622-StHA mainly identified ribosomal proteins of the large subunit (RPL) and 60S trans-acting factors like NMD3, DUSP12, LSG1 and PA2G4(ARX1), which all possess well studied homologs in yeast (Fig. 1A and Table S1). Notably, while yeast Rei1 is exclusively cytoplasmic (46), ZNF622 additionally localizes to nucleoli and accumulates in the nucleoplasm upon inhibition of the exportin CRM1 (Fig. S1). ZNF622 can thus be expected to associate with both early and late pre-60S particles.

Interestingly, several proteins isolated by TAP of ZNF622 have no homologs in lower eukaryotes (Table S1). Two of these proteins are NF45(ILF2) and NF90(ILF3), which were prominent hits within their bands (peptide coverage of 19% and 20%, respectively). NF45 and NF90 were also present in TAPs of MRTO4 and PA2G4, which also co-purify pre-60S particles (data not shown). To analyze whether NF45 and NF90 associate with 60S-sized particles, we determined their sedimentation behaviour by sucrose gradient centrifugation of HeLa cell extract. Western blot analysis revealed that both NF45 and NF90 were detected in the dense fractions of the gradient and partially co-sedimented with 60S-sized complexes in fractions containing the 60S trans-acting factor LSG1 (Fig. 1B). Both factors were also present in the bottom fraction of the gradient associated with particles heavier than 60S, similar to what has been previously observed in HeLa and HEK293 cells (10, 15). The longer isoform of ILF3, termed NF110, was only detected at the top of the gradient (Fig. 1B), suggesting that it is only present as a free protein or as part of smaller complexes but not associated with ribosomal subunits.

To assess whether the association of NF45/NF90 is specific for pre-60S particles, we performed TAP using either ZNF622 or the 40S trans-acting factors LTV1 and PNO1 as baits, which purify pre-40S particles (37). Western blot analysis revealed that NF45 and NF90 specifically co-purify with pre-60S particles but not with pre-40S particles (Fig. 1C). Consistent with the sucrose gradient analysis, NF110 was not co-purified by any of the TAPs (Fig. 1C).

NF45 and NF90 are enriched in nucleoli

Both NF45 and NF90 were identified as components of the nucleolar proteome (29, 30). Moreover, it has previously been reported that NF90 is able to shuttle between the nucleus and the cytoplasm and that its subcellular localization is dependent on tissue type and cell cycle stage (47, 48). Cell fractionation of HeLa cells showed that NF45 and NF90/NF110 are nuclear at steady state (Fig. 2A). Immunofluorescence analysis revealed a strong enrichment of NF45 in nucleoli whereas an antibody recognizing both NF90 and NF110 (α-ILF3) displayed a signal only slightly enriched at nucleoli (Fig. 2B).

To distinguish between the localization of NF90 and NF110, we used an antibody that specifically recognizes the unique C terminus of NF110, which showed that endogenous NF110 is localized to the nucleoplasm and is excluded from nucleoli (Fig. 2B). Further, we generated tagged versions of NF90 and NF110, and transiently transfected them into HeLa cells. N- and C-terminally tagged NF90 are enriched in nucleoli, similar to endogenous NF45 and the nucleolar trans-acting factor RLP24/RSL24D1 (Fig. 2B,C,D). In contrast, HASt-tagged NF110 is distributed more evenly throughout the nucleus, with only a small fraction of cells showing nucleolar enrichment of NF110 at higher expression levels (Fig. 2C,D). This suggests a putative role for NF45 and NF90 in nucleoli, the site of ribosome biogenesis.

The dsRBDs of NF90 are required for its association with pre-60S particles

To verify the association of NF90 with pre-60S particles, we generated a HEK293 cell line that inducibly expresses HASt-NF90 and performed TAP.

Mass spectrometry (Fig. 3A and Table S2) as well as Western blot analyses (Fig. 3B) showed that HASt-NF90 efficiently co-purified NF45, RPLs and 60S trans-acting factors such as ZNF622, PA2G4 and MRTO4 (Table S2). Notably, some late assembling RPL proteins and RPS proteins were also identified, consistent with previous data describing association of NF45 and NF90 with mono- and polysomes as well as with cytoplasmic mRNP granules containing mature 40S subunits (10, 15, 49). Supporting the latter, IGF2BP1/IMP1, which was used to purify these granules, also co-purified with HASt-NF90 (Table S2).

It is conceivable that NF90 interacts directly with rRNA via its dsRBDs. Another mode of binding to pre-60S could be mediated through its binding partner NF45, which would render the DZF domain of NF90 essential for pre-60S association. To elucidate how NF90 interacts with pre-60S particles, we generated HASt-tagged truncations of NF90 that either lacked only the C terminal domain (aa 1-602; ΔC), both dsRBDs and the nuclear localization signal (NLS) (aa 1-381; ΔdsRBD; (5)) or only the dsRBDs (aa 1-397; ΔdsRBD+NLS) (Fig. 4A). In addition, an NF90 mutant was generated in which two conserved amino acids at the dimerization interface with NF45 were mutated to amino acids of the opposite charge (E312R, R323E; DZFmut), analogous to the D308R, R319E mutations in murine NF45, which disrupt binding to NF90 (19). To see whether these constructs differ in their subcellular localization, they were transiently expressed as HASt-tagged fusion proteins in HeLa cells. While all proteins were expressed at similar levels (Fig. 4B), their localization differed greatly. Full-length NF90 as well as NF90ΔC were enriched in nucleoli (Fig. 4C). The DZF mutant of NF90 also predominantly localized to nucleoli, suggesting that binding to NF45 is not required for nucleolar localization of NF90 (Fig. 4C). In contrast, NF90ΔdsRBD localized to the cytoplasm and nucleoplasm but not to nucleoli. NF90ΔdsRBD+NLS was efficiently imported into the nucleus but still excluded from nucleoli (Fig. 4C), demonstrating that the dsRBDs of NF90 are required for its nucleolar localization. Notably, C-terminal truncation constructs lacking just the second dsRBD (NF90 1-528 and NF90 1-467) also failed to localize to

nucleoli, indicating that the first dsRBD alone is insufficient to promote nucleolar localization (Fig. S2).

To investigate whether the subcellular localization correlates with the ability of NF90 to associate with pre-60S particles, we generated HEK293 cell lines inducibly expressing NF90 derivatives and performed TAP followed by silver staining and Western blot analysis. Indeed, the dsRBD truncation mutants (ΔdsRBD and ΔdsRBD+NLS), which failed to localize to nucleoli, did not bind to pre-60S particles (Fig. 5A,B), whereas binding to NF45 was unaffected. The elution pattern for NF90ΔC was very similar to wild-type NF90. In contrast, the DZF mutant was not able to bind NF45, as expected, but still co-purified pre-60S particles (Fig. 5A,B), albeit with a lower yield. This is due to reduced expression of this construct, consistent with NF45 and NF90/110 influencing each other's stability (26). Taken together, these data demonstrate that association of NF90 with pre-60S depends on its dsRBDs but not on NF45.

Depletion of NF45 or NF90 leads to 60S biogenesis defects and changed nucleolar morphology

Having established the interaction of NF45 and NF90 with pre-60S ribosomal particles, we addressed their potential involvement in ribosome biogenesis. For this, we used a 60S subunit biogenesis reporter HeLa cell line in which RPL29(eL29)-GFP can be expressed in a tetracycline-inducible manner (36). Downregulation of NF45 or NF90/NF110 by siRNA treatment led to decreased RPL29-GFP levels in the cytoplasm of the reporter cells (Fig. 6A), indicative of a 60S biogenesis defect. This observation was confirmed in HeLa cells expressing an RPL26(uL24)-GFP reporter (Fig. 6A). Depletion of NF90/NF110 also decreased protein levels of NF45 as previously reported (26), and, to a lesser extent, vice versa (Fig. 6B).

To further validate the observed defects in 60S subunit synthesis, we performed sucrose gradient analysis of control cells or cells depleted of NF45 to analyze changes in the levels of pre-60S subunits (Fig. 6C, D). We used sedimentation of the 60S trans-acting factor LSG1 as readout, which has been implicated in the loading of RPL10(uL16) onto newly made 60S subunits

400 in the cytoplasm (50, 51). This analysis showed that less LSG1 sediments in
401 the (pre)-60S peak when NF45 was depleted (Fig. 6C), consistent with
402 reduced levels of late pre-60S subunits.
403 We also examined effects on 40S subunit biogenesis using an RPS2(uS5)-
404 YFP expressing HeLa cell line (Fig. S3). This analysis revealed a slight effect
405 on 40S biogenesis, manifesting by nucleoplasmic accumulation of RPS2-YFP
406 in some cells, especially upon depletion of NF45. This is consistent with our
407 previous finding that impaired 60S biogenesis impinges on 40S subunit
408 synthesis (36). An example of this phenotype is shown for downregulation of
409 the bona fide 60S trans-acting factor AAMP (Fig. S3,(36)).
410 Strikingly, cells depleted of NF45 or NF90/NF110 contained fewer and larger
411 nucleoli displaying a distinct, almost circular shape marked by the reporter
412 protein (Fig. 6A). These changes in nucleolar number and morphology were
413 also detected by immunofluorescence of nucleolar markers in HeLa cells not
414 carrying the reporter construct (Fig. 7A). The analyzed nucleolar proteins
415 included upstream binding factor (UBF), fibrillarin (FBL) and nucleophosmin
416 (NPM), which serve as markers for different nucleolar subdomains (the fibrillar
417 center, the dense fibrillar component and the granular component,
418 respectively). The immunofluorescence analysis of these factors, however,
419 showed no indication for a disruption of one of these nucleolar subdomains.
420 To quantify the observed changes in nucleolar shape, we developed an image
421 analysis tool that can automatically detect nucleoli and measure nucleolar
422 circularity as the ratio between the length of the major and minor axis of each
423 nucleolus. Accordingly, a perfectly round nucleolus would theoretically
424 possess major/minor axis ratio of 1, whereas larger numbers are indicative of
425 deviations from a perfect spherical shape.
426 In control cells, the mean ratio of major/minor axes was 1.38, whereas in
427 NF45 and NF90/NF110 depleted cell the ratio decreased significantly to 1.19
428 and 1.18, respectively (Fig. 7B), demonstrating that nucleoli possess a more
429 elongated structure in control cells and have a rounder form upon loss of
430 NF45 or NF90/NF110. Importantly, the round nucleolar shape phenotype
431 induced by depletion of NF90/NF110 could be rescued by expression of an
432 siRNA-insensitive HASt-NF90 construct (Fig. S4), ruling out an RNAi off-
433 target effect. Interestingly, the same changes in nucleolar shape and numbers

were observed upon depletion of the 60S trans-acting factors ZNF622 and PES1 (Fig. 7 C,D). In contrast, downregulation of RPL11/uL5 did not lead to rounder nucleoli (Fig. S6C).

The decrease in RPL29-GFP signal in the cytoplasm might be explained by a failure in nuclear maturation or export of pre-60S subunits. Export of human pre-60S particles is dependent on the exportins CRM1(XPO1) and XPO5(EXP5) (36, 52, 53). Interestingly, NF90 can form an RNA-dependent complex with XPO5 (54, 55). Both proteins mutually increase their affinity for dsRNA targets (56). To test whether NF45 and NF90 contribute to the recruitment of pre-60S export receptors, we assessed whether pre-60S particles lacking NF45 and NF90 are able to bind XPO5. However, we could not observe diminished binding of either XPO5 or CRM1 to pre-60S subunits *in vitro* after co-depletion of NF45 and NF90 (Fig. S5), suggesting a ribosome biogenesis defect upon NF45/NF90 depletion that is distinct from export factor recruitment. Further, depletion of XPO5 did not phenocopy the nucleolar alterations caused by downregulation of NF45 and NF90/NF110 (Fig. 7C, D), indicating that defective subunit export does not cause nucleolar rounding.

Ribosome maturation is intricately linked to the multistep pathway of rRNA processing, in which successive cleavage of the human 47S rRNA precursor leads to mature 18S, 28S and 5.8S rRNAs (Fig. S6A). To test whether the NF45/NF90 heterodimer is involved in rRNA processing, we performed siRNA-mediated depletion experiments in HeLa cells and analyzed pre-ribosomal RNAs by Northern blotting using two different probes specifically recognizing precursors of 18S and 28S rRNA (5' ITS1 and ITS2 probe, respectively (42)) (Fig. S6A). However, we did not observe an accumulation of a specific rRNA precursor to 18S or 28S rRNA upon NF45 and/or NF90/NF110 depletion, in contrast to depletion of RPL11 (Fig. S6B). Also pulse-chase analysis of rRNA maturation failed to reveal clear changes in pre-rRNA transcription and processing upon NF45/NF90 depletion (data not shown). Likewise, pre-rRNA FISH using a probe directed to the 5' ETS of human pre-rRNA (44) showed no changes in the apparent levels of 47S pre-rRNA as compared to depletion of the RNA POL I subunit POLR1A (Fig. S6D). These FISH experiments, however, clearly recapitulated the nucleolar rounding induced by downregulation of the NF45/NF90 heterodimer.

Collectively, these data show that the depletion of NF45 and NF90 causes nucleolar rounding and a 60S biogenesis defect without obvious effects on nucleolar rRNA processing.

NF45/NF90 co-depletion leads to RPL11-dependent p21 increase

It is well established that defects in early steps of ribosome biogenesis generate a free pool of RPL11/uL5 and RPL5/uL18, which together with 5S rRNA bind to and inhibit the E3 ubiquitin ligase HDM2, leading to p53 stabilization and the induction of p53 target genes (57-60). Interestingly, depletion of NF45 and NF90 in HeLa cells has been previously shown to increase the levels of p53 accompanied by an upregulation of the cyclin-dependent kinase inhibitor p21(CDKN1A, CIP1) (61). Consistent with these published data, we observed a slight increase in p53 levels and an accumulation of p21 when we depleted NF45 or NF90/110 by RNAi in HeLa cells (Fig. 8A).

HeLa cells are known to fail cell cycle arrest upon p21 induction as a consequence of the inhibitory action of the human papilloma virus E7 protein on p21 and pRb (62-64). Yet, nucleoli are known to fuse in the G1 phase of the cell cycle (65, 66), and a G1 arrest might explain the observed nucleolar changes upon NF45/NF90 depletion. To test whether downregulation of NF45 and/or NF90 affects the cell cycle, we performed cell cycle analysis after RNAi. Flow cytometry revealed that, despite p21 induction, the cell cycle profiles of NF45 or NF90/110-depleted HeLa cells were not significantly changed (Fig. 8B,C). These results indicate that the changes in nucleolar morphology observed upon downregulation of NF45 or NF90/110 (Fig. 7A,B; Fig. 8D,E) are not the consequence of a G1 arrest. To exclude this possibility more directly, we arrested cells at the G1-S transition by a double thymidine block and analyzed nucleolar morphology (Fig. S7). Quantitative analysis of nucleolar circularity revealed only very minor changes in nucleolar morphology, in contrast to the severe phenotype observed upon NF45 or NF90/110 depletion. Also a prolongation of the second phase of the double thymidine block by another 8 hours did not induce further nucleolar rounding (F. Wandrey and U. Kutay, unpublished).

To finally test whether the increased levels of p53 and p21 are due to 'nucleolar stress' caused by a defect in ribosome synthesis, we analyzed whether loss of RPL11 can impede upregulation of p53 and p21 upon NF45 or NF90/NF110 depletion. When we downregulated NF45 or NF90/NF110 by RNAi in U2OS cells there was an increase in p53 levels accompanied by a marked induction of p21 (Fig. 8F). Strikingly, upregulation of p21 upon depletion of NF45 or NF90/NF110 was prevented by co-depletion of RPL11, suggesting that an increased free pool of RPL11 is required for p21 induction.

DISCUSSION

Many trans-acting factors support the assembly, processing and maturation of ribosomal subunits. In this study, we identified NF45 and NF90 as two novel trans-acting factors that support 60S subunit biogenesis in human cells. Our data show that the NF45/NF90 heterodimer is associated with pre-60S particles. We further demonstrate that NF45 and NF90 localize to nucleoli, the site of rRNA transcription and initial ribosome assembly steps. Both nucleolar localization and pre-60S association of NF90 depend on its dsRBDs.

TAP experiments using an NF90 mutant deficient in interaction with NF45 revealed that binding of NF90 to NF45 is dispensable for association of NF90 with pre-60S particles. However, depletion of NF45 and NF90 similarly affected ribosome biogenesis, revealed by the loss of cytoplasmic accumulation of a 60S subunit biogenesis reporter. These data indicate that even though NF90 can bind to pre-60S subunits without NF45, NF90 alone is insufficient to support the ribosome biogenesis pathway. One possible reason for the mutual need of both subunits is that they influence each other's stability (26). However, over the course of our RNAi experiments, depletion of NF45 affected the levels of NF90 much less severely than vice versa, supporting a more direct requirement of NF45 for 60S biogenesis. Consistent with the role of the NF45/NF90 heterodimer in ribosome biogenesis, downregulation of either subunit or the heterodimer caused an RPL11-dependent induction of the p53 target gene p21.

The extended isoform of ILF3, NF110, is neither part of pre-60S subunits nor enriched in nucleoli, although NF110 possesses dsRBDs identical to NF90. We suspect that the distinct C-terminal domain of NF110 contains interaction motifs that lead to its sequestration in the nucleoplasm, in accordance with previous reports describing a role of NF110 in POL II transcription and association with chromatin (26-28).

In addition to affecting the biogenesis of 60S ribosomal particles, depletion of NF45 or NF90 led to changes in nucleolar size, number and morphology. Cells contained fewer but larger nucleoli that adopted a striking spherical shape. Emerging concepts posit that intracellular organization of RNA-containing subdomains such as nucleoli, Cajal bodies, P-bodies and stress

544 granules is based on molecular crowding effects leading to phase separation
545 of liquids accompanied by liquid droplet formation (67-69). In support of liquid
546 phase separation playing a role in nucleolar organization, it has been shown
547 that the size and shape of *Xenopus laevis* oocyte nucleoli depend on their
548 liquid-like behavior and surface tension (70).
549 But what is the molecular mechanism underlying the nucleolar shape changes
550 upon depletion of NF45 or NF90? It is conceivable that a failure in nucleolar
551 maturation and exit of pre-60S particles, as induced by downregulation of
552 NF45/NF90, leads to increased molecular crowding in nucleoli accompanied
553 by a clearer phase separation from the surrounding nucleoplasm. In this
554 scenario, the formation of fewer but larger nucleoli would be a consequence
555 of nucleolar fusion occurring as a result of coalescence of phase droplets.
556 Indeed, in preliminary experiments, we have observed such fusion events
557 upon NF45 depletion (unpublished observation). Our experiments further
558 indicate that the observed changes in shape are unlikely to be a consequence
559 of cell cycle defects since we neither observed a cell cycle arrest upon
560 NF45/NF90 depletion nor did an induced cell cycle arrest cause similar
561 changes in nucleolar morphology.
562 Notably, not all ribosomal proteins and 60S trans-acting factors cause the
563 same change in nucleolar architecture upon depletion. XPO5 knockdown, for
564 instance, which causes nucleoplasmic accumulation of pre-60S particles by
565 impairing pre-60S nuclear export (36), does not cause nucleolar rounding
566 (Fig. 6). In contrast, depletion of other nucleolar pre-60S biogenesis factors
567 such as PES1 and ZNF622 led to nucleolar rounding as observed for NF45
568 and NF90 depletion. Similarly, rounding up of nucleoli has been reported
569 previously for depletion of RPS6 (71) and NOL11, a component of the SSU
570 processome (72). Collectively, these observations may suggest that
571 accumulation of ribosome assembly intermediates or byproducts caused by
572 nucleolar ribosome biogenesis defects is a cause for the ball-shaped nucleoli.
573 Curiously, Northern blot analysis failed to reveal an accumulation of any 28S
574 rRNA precursors upon depletion of NF45 or NF90. The lack of accumulation
575 of distinct rRNA precursors upon depletion of NF45 or NF90 suggests that
576 rRNA processing is not impaired. However, we cannot fully exclude that
577 assembly-defective particles are rapidly eliminated by degradation. Yet, the

lack of processing defects could also indicate that nucleolar 60S biogenesis is affected at a very late step, subsequent to nucleolar steps of 28S rRNA processing, perhaps just prior to or at the release of pre-60S subunits into the nucleoplasm.

The DZF domains of NF45 and NF90 possess structural similarities to template-free nucleotidyltransferases such as poly(A) polymerases, TUTases or the CCA adding enzyme (19). While both NF45 and NF90 have likely lost enzymatic activity, NF45 is able to bind nucleotides *in vitro* (19). It is therefore tempting to speculate that the NF45/NF90 heterodimer, recruited to pre-60S subunits by help of NF90's dsRBDs, is able to recognize the terminal ends of (pre)-rRNAs protruding from the 60S subunit surface by the two juxtaposed DZF domains. This binding might constitute a quality control or licensing step required to foster final nucleolar pre-60S remodeling steps or exit from the nucleolus.

The NF45/NF90 heterodimer has been previously implicated in a plethora of cellular pathways (5-17). The involvement of NF45/NF90 in ribosome synthesis identified here adds a very basic cellular pathway to its functional repertoire, and could well explain why NF90 is essential in vertebrates. However, as for other multifunctional factors, it will be a challenge to disentangle these diverse roles and to distinguish direct from indirect effects by identifying the underlying molecular mechanism of NF45/NF90 function. It can be expected that insights into the role of the DZF domains beyond promoting heterodimer formation will be crucial for this endeavor.

Acknowledgments

We thank the members of the Kutay lab for helpful discussions and Caroline Ashiono for excellent technical assistance. Microscopy was performed on instruments of the ETHZ Microscopy Center (ScopeM). Flow cytometry experiments were supported by ETHZ Flow Cytometry Facility. This work was funded by a grant of the Swiss National Science Foundation (31003A_144221) to U.K..

FIGURE LEGENDS

FIG 1 NF45 and NF90, but not NF110, are components of pre-60 particles.
(A) HEK293 cells expressing ZNF622-StHA were used for tandem-affinity purification (TAP). The purified proteins were analyzed by SDS-PAGE followed by Coomassie staining and mass-spectrometry analysis of excised bands (Table S1). Proteins detected with the highest peptide numbers are listed on the right. Grey protein names indicate proteins for which there are either no yeast homologs or yeast homologs that have not been implicated in ribosome biogenesis. TAP of ZNF622-StHA purifies pre-60S particles as well as NF45 and NF90.
(B) HeLa cell extract was centrifuged on a 10%-45% sucrose gradient. Cell extract (Input) and gradient fractions were analyzed by Western blotting using the indicated antibodies. Note that the α-ILF3 antibody recognizes both the NF90 and the NF110 isoform of ILF3. Fractions containing 40S and 60S particles are indicated at the bottom. NF45 and NF90 co-migrate in fractions containing 60S particles whereas NF110 is present at the top of the gradient.
(C) TAP of HEK293 cells expressing the 60S trans-acting factor ZNF622-StHA or the 40S trans-acting factors HASt-LTV1 or HASt-PNO1 was performed. Cleared cell extracts (Input) and eluted proteins (Eluate) were analyzed by Western blotting using the indicated antibodies. NF45 and NF90, but not NF110, were co-purified by ZNF622 TAP, but were not present in the eluate samples obtained by LTV1 or PNO1 TAP.

FIG 2 NF45 and NF90 localize to the nucleus and are enriched in nucleoli.
(A) Extract from HeLa cells was fractionated and equal volumes of total cells, cytoplasmic extract and the pellet containing the nucleus were analyzed by Western blotting using the indicated antibodies. NF45 and NF90 are exclusively present in the nuclear fraction at steady state.
(B) Localization of NF45 and NF90/NF110 in HeLa cells was analyzed by immunofluorescence with the indicated antibodies. NF45 is enriched in nucleoli whereas NF110 is predominantly localized to the nucleoplasm. Scale bar, 20 µm.

(C) HeLa cells were transiently transfected with N- and C-terminally HASt-tagged NF90 or NF110. The subcellular localization of tagged proteins was detected by immunofluorescence using an anti-HA antibody. Nucleoli were visualized by co-immunofluorescence against RLP24. Scale bar, 20 µm.
(D) Western blot analysis of cells from (C) using the indicated antibodies to monitor expression levels of transfected constructs.

FIG 3 NF90 TAP co-purifies pre-60S particles.
TAP was performed using HEK293 cells expressing either HASt-NF90 or HASt-GFP (negative control) as bait.
(A) Eluted proteins were analyzed by SDS-PAGE followed by silver staining (pictured) or Coomassie blue staining. Bands visible by Coomassie blue staining were excised and analyzed by mass spectrometry (Table S2). The proteins with the highest number of peptides detected are indicated on the right. Grey protein names indicate proteins for which there are either no yeast homologs or yeast homologs that have not been implicated in ribosome biogenesis. Baits are marked with an asterisk.
(B) Western blot analysis of the TAP experiment in (A) with the indicated antibodies. NF90 co-purifies NF45, ribosomal proteins of the 60S subunit as well as 60S, but not 40S trans-acting factors.

FIG 4 The dsRBDs of NF90 are required for nucleolar localization.
(A) Scheme of generated NF90 truncations/mutants. Full-length NF90 possesses an N-terminal DZF domain (green) with which it dimerizes with NF45, a nuclear localization signal (NLS, depicted in blue) and two dsRBD domains (orange). Amino acid numbers indicate the positions of domains and the length of each NF90 truncation. The two mutated amino acid residues for the DZF mutant are labeled in red.
(B) The N-terminally HASt-tagged NF90 constructs from (A) were transiently transfected into HeLa cells for 24 h. Cells were harvested and analyzed by Western blotting using the indicated antibodies.
(C) Cells transfected as in (B) were fixed and analyzed by immunofluorescence using the indicated antibodies. Scale bar, 20 µm.

FIG 5 The dsRBDs of NF90 are required for association with pre-60S particles.
(A) TAP using HEK293 cell lines inducibly expressing the indicated HASt-tagged NF90 constructs and HASt-GFP as negative control. Eluates were analyzed by SDS-PAGE followed by silver staining (A) or Western blotting (B) using the indicated antibodies. Baits are marked with asterisks. NF90 truncations lacking the dsRBDs do not co-purify pre-60S particles.

FIG 6 NF45/NF90 depletion leads to a ribosome biogenesis defect.
(A) HeLa cells expressing RPL29-GFP or RPL26-GFP under a tetracycline-dependent promoter were treated with either control siRNA (si-control) or siRNAs against NF45 or NF90/110 for 72 h. Cells were fixed and analyzed by fluorescence microscopy. Scale bar, 20 µm.
(B) Western blot analysis to control for downregulation of NF45 and NF90 in RPL29-GFP expressing cells from (A) using the indicated antibodies.
(C) HeLa K cells were treated with either control siRNA (si-control) or siRNAs against NF45 for 72 h. Cell extracts were separated by centrifugation on a linear 10%-45% sucrose gradient. Cell extract (Input) and gradient fractions were analyzed by Western blotting using the indicated antibodies. Fractions containing 40S and 60S particles are indicated at the bottom. Note that binding of LSG1 to pre-60S particles is diminished upon NF45 depletion.
(D) To confirm NF45 downregulation, cell extracts from (C) were analyzed by Western blotting using the indicated antibodies.

FIG 7 NF45/NF90 depletion leads to altered nucleolar morphology.
(A) HeLa K cells were treated with either control siRNA (si-control) or siRNAs against NF45 or NF90/110 for 72 h. Cells were fixed and analyzed by IF using the indicated antibodies. Larger spaces between panels separate independent experiments. Scale bar, 20 µm.
(B) Quantification of nucleolar shape of cells from three independent experiments using the α-eIF6 readout. Error bars indicate standard deviation. Statistically significant differences from control cells, determined by a t-test, are indicated (** P value ≤0.01)

(C) HeLa cells were transfected with the indicated siRNAs for 72 h and analyzed by immunofluorescence using an antibody against eIF6. Scale bar, 20 µm.
(D) Quantification of nucleolar shape from three independent experiments analogous to (B). (** P value ≤0.01; * P value ≤0.05).

FIG 8 Depletion of NF45 and NF90 does not cause cell cycle arrest in HeLa cells but leads to RPL11-dependent p21 induction.
(A) HeLa cells were treated with the indicated siRNAs for 72 h and analyzed by Western blotting with the indicated antibodies.
(B) HeLa cells were treated with the indicated siRNAs for 72 h and analyzed by flow cytometry. Three independent experiments were quantified and the percentage of cells in G1 for each condition is shown with standard deviation. A t-test was performed to determine significant differences (ns = not significant).
(C) Flow cytometry histograms of one representative experiment from (B). Cell cycle stages are indicated in the first histogram panel.
(D) Immunofluorescence analysis of one of the experiments in (B) using an antibody against eIF6. Scale bar, 20 µm.
(E) Quantification of nucleolar shape of cells from (D). Per condition, > 300 nucleoli were analyzed. Bars are shown with standard deviation and a t-test was performed to determine significant differences (*** = P value < 0.001).
(F) U2OS cells were treated with the indicated siRNAs for 72 h and analyzed by Western blotting with the indicated antibodies.

REFERENCES

1. **Corthésy B, Kao PN.** 1994. Purification by DNA affinity chromatography of two polypeptides that contact the NF-AT DNA binding site in the interleukin 2 promoter. J. Biol. Chem. **269:**20682-20690.
2. **Kao PN, Chen L, Brock G, Ng J, Kenny J, Smith AJ, Corthésy B.** 1994. Cloning and expression of cyclosporin A- and FK506-sensitive nuclear factor of activated T-cells: NF45 and NF90. J. Biol. Chem. **269:**20691-20699.
3. **Marcoulatos P, Koussidis G, Mamuris Z, Velissariou V, Vamvakopoulos NC.** 1996. Mapping interleukin enhancer binding factor 2 gene (ILF2) to human chromosome 1 (1q11-qter and 1p11-p12) by polymerase chain reaction amplification of human-rodent somatic cell hybrid DNA templates. J. Interferon Cytokine Res. **16:**1035-1038.
4. **Zhao G, Shi L, Qiu D, Hu H, Kao PN.** 2005. NF45/ILF2 tissue expression, promoter analysis, and interleukin-2 transactivating function. Exp. Cell Res. **305:**312-323.
5. **Reichman TW, Muñiz LC, Mathews MB.** 2002. The RNA binding protein nuclear factor 90 functions as both a positive and negative regulator of gene expression in mammalian cells. Mol. Cell. Biol. **22:**343-356.
6. **Shi L, Godfrey WR, Lin J, Zhao G, Kao PN.** 2007. NF90 regulates inducible IL-2 gene expression in T cells. J. Exp. Med. **204:**971-977.
7. **Kiesler P, Haynes PA, Shi L, Kao PN, Wysocki VH, Vercelli D.** 2010. NF45 and NF90 regulate HS4-dependent interleukin-13 transcription in T cells. J. Biol. Chem. **285:**8256-8267.
8. **Shamanna RA, Hoque M, Lewis-Antes A, Azzam EI, Lagunoff D, Pe'ery T, Mathews MB.** 2011. The NF90/NF45 complex participates in DNA break repair via nonhomologous end joining. Mol. Cell. Biol. **31:**4832-4843.
9. **Ting NS, Kao PN, Chan DW, Lintott LG, Lees-Miller SP.** 1998. DNA-dependent protein kinase interacts with antigen receptor response element binding proteins NF90 and NF45. J. Biol. Chem. **273:**2136-2145.
10. **Pfeifer I, Elsby R, Fernandez M, Faria PA, Nussenzveig DR, Lossos IS, Fontoura BMA, Martin WD, Barber GN.** 2008. NFAR-1 and -2 modulate translation and are required for efficient host defense. Proc. Natl. Acad. Sci. U. S. A. **105:**4173-4178.
11. **Masuda K, Kuwano Y, Nishida K, Rokutan K, Imoto I.** 2013. NF90 in posttranscriptional gene regulation and microRNA biogenesis. International journal of molecular sciences **14:**17111-17121.
12. **Sakamoto S, Aoki K, Higuchi T, Todaka H, Morisawa K, Tamaki N, Hatano E, Fukushima A, Taniguchi T, Agata Y.** 2009. The NF90-NF45 complex functions as a negative regulator in the microRNA processing pathway. Mol. Cell. Biol. **29:**3754-3769.
13. **Isken O, Grassmann CW, Sarisky RT, Kann M, Zhang S, Grosse F, Kao PN, Behrens S-E.** 2003. Members of the NF90/NFAR protein group are involved in the life cycle of a positive-strand RNA virus. EMBO J. **22:**5655-5665.
14. **Krasnoselskaya-Riz I, Spruill A, Chen Y-W, Schuster D, Teslovich T, Baker C, Kumar A, Stephan DA.** 2002. Nuclear factor 90 mediates activation of the cellular antiviral expression cascade. AIDS Res. Hum. Retrovir. **18:**591-604.
15. **Merrill MK, Gromeier M.** 2006. The double-stranded RNA binding protein 76:NF45 heterodimer inhibits translation initiation at the rhinovirus type 2 internal ribosome entry site. J. Virol. **80:**6936-6942.

16. **Shabman RS, Leung DW, Johnson J, Glennon N, Gulcicek EE, Stone KL, Leung L, Hensley L, Amarasinghe GK, Basler CF.** 2011. DRBP76 associates with Ebola virus VP35 and suppresses viral polymerase function. J. Infec. Dis. **204 Suppl 3:**S911-918.
17. **Wang P, Song W, Mok BW-Y, Zhao P, Qin K, Lai A, Smith GJD, Zhang J, Lin T, Guan Y, Chen H.** 2009. Nuclear factor 90 negatively regulates influenza virus replication by interacting with viral nucleoprotein. J. Virol. **83:**7850-7861.
18. **Shi L, Zhao G, Qiu D, Godfrey WR, Vogel H, Rando TA, Hu H, Kao PN.** 2005. NF90 regulates cell cycle exit and terminal myogenic differentiation by direct binding to the 3'-untranslated region of MyoD and p21WAF1/CIP1 mRNAs. J. Biol. Chem. **280:**18981-18989.
19. **Wolkowicz UM, Cook AG.** 2012. NF45 dimerizes with NF90, Zfr and SPNR via a conserved domain that has a nucleotidyltransferase fold. Nucleic Acids Res. **40:**9356-9368.
20. **Barber GN.** 2009. The NFAR's (nuclear factors associated with dsRNA): evolutionarily conserved members of the dsRNA binding protein family. RNA Biol. **6:**35-39.
21. **Langland JO, Kao PN, Jacobs BL.** 1999. Nuclear factor-90 of activated T-cells: A double-stranded RNA-binding protein and substrate for the double-stranded RNA-dependent protein kinase, PKR. Biochemistry **38:**6361-6368.
22. **Liao HJ, Kobayashi R, Mathews MB.** 1998. Activities of adenovirus virus-associated RNAs: purification and characterization of RNA binding proteins. Proc. Natl. Acad. Sci. U. S. A. **95:**8514-8519.
23. **Patel RC, Vestal DJ, Xu Z, Bandyopadhyay S, Guo W, Erme SM, Williams BR, Sen GC.** 1999. DRBP76, a double-stranded RNA-binding nuclear protein, is phosphorylated by the interferon-induced protein kinase, PKR. J. Biol. Chem. **274:**20432-20437.
24. **Duchange N, Pidoux J, Camus E, Sauvaget D.** 2000. Alternative splicing in the human interleukin enhancer binding factor 3 (ILF3) gene. Gene **261:**345-353.
25. **Saunders LR, Jurecic V, Barber GN.** 2001. The 90- and 110-kDa human NFAR proteins are translated from two differentially spliced mRNAs encoded on chromosome 19p13. Genomics **71:**256-259.
26. **Guan D, Altan-Bonnet N, Parrott AM, Arrigo CJ, Li Q, Khaleduzzaman M, Li H, Lee C-G, Peery T, Mathews MB.** 2008. Nuclear factor 45 (NF45) is a regulatory subunit of complexes with NF90/110 involved in mitotic control. Mol. Cell. Biol. **28:**4629-4641.
27. **Reichman TW, Mathews MB.** 2003. RNA binding and intramolecular interactions modulate the regulation of gene expression by nuclear factor 110. RNA (New York, NY) **9:**543-554.
28. **Reichman TW, Parrott AM, Fierro-Monti I, Caron DJ, Kao PN, Lee C-G, Li H, Mathews MB.** 2003. Selective regulation of gene expression by nuclear factor 110, a member of the NF90 family of double-stranded RNA-binding proteins. J. Mol. Biol. **332:**85-98.
29. **Ahmad Y, Boisvert F-M, Gregor P, Cobley A, Lamond AI.** 2009. NOPdb: Nucleolar Proteome Database--2008 update. Nucleic Acids Res. **37:**D181-184.
30. **Jarboui MA, Wynne K, Elia G, Hall WW, Gautier VW.** 2011. Proteomic profiling of the human T-cell nucleolus. Mol. Immunol. **49:**441-452.
31. **Fromont-Racine M, Senger B, Saveanu C, Fasiolo F.** 2003. Ribosome assembly in eukaryotes. Gene **313:**17-42.
32. **Henras AK, Soudet J, Gérus M, Lebaron S, Caizergues-Ferrer M, Mougin A, Henry Y.** 2008. The post-transcriptional steps of eukaryotic ribosome biogenesis. Cellular and molecular life sciences : CMLS **65:**2334-2359.

33. **Kressler D, Hurt E, Bassler J.** 2010. Driving ribosome assembly. Biochimica Et Biophysica Acta-Molecular Cell Research **1803:**673-683.
34. **Tschochner H, Hurt E.** 2003. Pre-ribosomes on the road from the nucleolus to the cytoplasm. Trends Cell Biol. **13:**255-263.
35. **Lim YH, Charette JM, Baserga SJ.** 2011. Assembling a protein-protein interaction map of the SSU processome from existing datasets. PLoS One. **6:**e17701.
36. **Wild T, Horvath P, Wyler E, Widmann B, Badertscher L, Zemp I, Kozak K, Csucs G, Lund E, Kutay U.** 2010. A protein inventory of human ribosome biogenesis reveals an essential function of exportin 5 in 60S subunit export. PLoS Biol. **8:**e1000522.
37. **Wyler E, Zimmermann M, Widmann B, Gstaiger M, Pfannstiel J, Kutay U, Zemp I.** 2011. Tandem affinity purification combined with inducible shRNA expression as a tool to study the maturation of macromolecular assemblies. RNA (New York, NY) **17:**189-200.
38. **Zemp I, Wandrey F, Rao S, Ashiono C, Wyler E, Montellese C, Kutay U.** 2014. CK1delta and CK1epsilon are components of human 40S subunit precursors required for cytoplasmic 40S maturation. J. Cell Sci. **127:**1242-1253.
39. **Zemp I, Wild T, O'Donohue MF, Wandrey F, Widmann B, Gleizes PE, Kutay U.** 2009. Distinct cytoplasmic maturation steps of 40S ribosomal subunit precursors require hRio2. J. Cell Biol. **185:**1167-1180.
40. **Wyler E, Wandrey F, Badertscher L, Montellese C, Alper D, Kutay U.** 2014. The beta-isoform of the BRCA2 and CDKN1A(p21)-interacting protein (BCCIP) stabilizes nuclear RPL23/uL14. FEBS Lett. **588:**3685-3691.
41. **Lund E, Guttinger S, Calado A, Dahlberg JE, Kutay U.** 2004. Nuclear export of microRNA precursors. Science **303:**95-98.
42. **Rouquette J, Choesmel V, Gleizes P-E.** 2005. Nuclear export and cytoplasmic processing of precursors to the 40S ribosomal subunits in mammalian cells. EMBO J. **24:**2862-2872.
43. **Otsu Y.** 1979. A Threshold Selection Method from Gray-Level Histograms. IEEE Trans. Sys. Man. Cyber. **9:**62-66.
44. **Granneman S, Vogelzangs J, Luhrmann R, van Venrooij WJ, Pruijn GJ, Watkins NJ.** 2004. Role of pre-rRNA base pairing and 80S complex formation in subnucleolar localization of the U3 snoRNP. Mol. Cell. Biol. **24:**8600-8610.
45. **Hung NJ, Johnson AW.** 2006. Nuclear recycling of the pre-60S ribosomal subunit-associated factor Arx1 depends on Rei1 in Saccharomyces cerevisiae. Mol. Cell. Biol. **26:**3718-3727.
46. **Lebreton A, Saveanu C, Decourty L, Rain JC, Jacquier A, Fromont-Racine M.** 2006. A functional network involved in the recycling of nucleocytoplasmic pre-60S factors. J. Cell Biol. **173:**349-360.
47. **Neplioueva V, Dobrikova EY, Mukherjee N, Keene JD, Gromeier M.** 2010. Tissue type-specific expression of the dsRNA-binding protein 76 and genome-wide elucidation of its target mRNAs. PLoS One. **5:**e11710.
48. **Parrott AM, Walsh MR, Reichman TW, Mathews MB.** 2005. RNA binding and phosphorylation determine the intracellular distribution of nuclear factors 90 and 110. J. Mol. Biol. **348:**281-293.
49. **Jonson L, Vikesaa J, Krogh A, Nielsen LK, Hansen T, Borup R, Johnsen AH, Christiansen J, Nielsen FC.** 2007. Molecular composition of IMP1 ribonucleoprotein granules. Mol. Cell. Proteomics **6:**798-811.
50. **West M, Hedges JB, Chen A, Johnson AW.** 2005. Defining the order in which Nmd3p and Rpl10p load onto nascent 60S ribosomal subunits. Mol. Cell. Biol. **25:**3802-3813.

51. **Reynaud EG, Andrade MA, Bonneau F, Ly TB, Knop M, Scheffzek K, Pepperkok R.** 2005. Human Lsg1 defines a family of essential GTPases that correlates with the evolution of compartmentalization. BMC biology **3:**21.
52. **Trotta CR, Lund E, Kahan L, Johnson AW, Dahlberg JE.** 2003. Coordinated nuclear export of 60S ribosomal subunits and NMD3 in vertebrates. EMBO J. **22:**2841-2851.
53. **Thomas F, Kutay U.** 2003. Biogenesis and nuclear export of ribosomal subunits in higher eukaryotes depend on the CRM1 export pathway. J. Cell Sci. **116:**2409-2419.
54. **Brownawell AM, Macara IG.** 2002. Exportin-5, a novel karyopherin, mediates nuclear export of double-stranded RNA binding proteins. J. Cell Biol. **156:**53-64.
55. **Calado A, Treichel N, Müller E, Otto A, Kutay U.** 2002. Exportin-5-mediated nuclear export of eukaryotic elongation factor 1A and tRNA. EMBO J. **21:**6216-6224.
56. **Gwizdek C, Ossareh-Nazari B, Brownawell AM, Evers S, Macara IG, Dargemont C.** 2004. Minihelix-containing RNAs mediate exportin-5-dependent nuclear export of the double-stranded RNA-binding protein ILF3. J. Biol. Chem. **279:**884-891.
57. **Marechal V, Elenbaas B, Piette J, Nicolas JC, Levine AJ.** 1994. The ribosomal L5 protein is associated with mdm-2 and mdm-2-p53 complexes. Mol. Cell. Biol. **14:**7414-7420.
58. **Lohrum MAE, Ludwig RL, Kubbutat MHG, Hanlon M, Vousden KH.** 2003. Regulation of HDM2 activity by the ribosomal protein L11. Cancer Cell **3:**577-587.
59. **Donati G, Peddigari S, Mercer CA, Thomas G.** 2013. 5S ribosomal RNA is an essential component of a nascent ribosomal precursor complex that regulates the Hdm2-p53 checkpoint. Cell Rep. **4:**87-98.
60. **Sloan KE, Mattijssen S, Lebaron S, Tollervey D, Pruijn GJM, Watkins NJ.** 2013. Both endonucleolytic and exonucleolytic cleavage mediate ITS1 removal during human ribosomal RNA processing. J. Cell Biol. **200:**577-588.
61. **Shamanna RA, Hoque M, Pe'ery T, Mathews MB.** 2013. Induction of p53, p21 and apoptosis by silencing the NF90/NF45 complex in human papilloma virus-transformed cervical carcinoma cells. Oncogene **32:**5176-5185.
62. **Funk JO, Waga S, Harry JB, Espling E, Stillman B, Galloway DA.** 1997. Inhibition of CDK activity and PCNA-dependent DNA replication by p21 is blocked by interaction with the HPV-16 E7 oncoprotein. Genes Dev. **11:**2090-2100.
63. **Jones DL, Alani RM, Munger K.** 1997. The human papillomavirus E7 oncoprotein can uncouple cellular differentiation and proliferation in human keratinocytes by abrogating p21Cip1-mediated inhibition of cdk2. Genes Dev. **11:**2101-2111.
64. **Ruesch MN, Laimins LA.** 1997. Initiation of DNA synthesis by human papillomavirus E7 oncoproteins is resistant to p21-mediated inhibition of cyclin E-cdk2 activity. J. Virol. **71:**5570-5578.
65. **Savino TM, Gebrane-Younes J, De Mey J, Sibarita JB, Hernandez-Verdun D.** 2001. Nucleolar assembly of the rRNA processing machinery in living cells. J. Cell Biol. **153:**1097-1110.
66. **Yamauchi K, Yang M, Hayashi K, Jiang P, Yamamoto N, Tsuchiya H, Tomita K, Moossa AR, Bouvet M, Hoffman RM.** 2007. Imaging of nucleolar dynamics during the cell cycle of cancer cells in live mice. Cell Cycle **6:**2706-2708.
67. **Brangwynne CP.** 2013. Phase transitions and size scaling of membrane-less organelles. J. Cell Biol. **203:**875-881.

68. **Cho EJ, Kim JS.** 2012. Crowding-induced phase separation of Lennard-Jones particles: implications to nuclear structures in a biological cell. J. Phys. Chem. B. **116:**3874-3879.
69. **Aumiller WM, Jr., Davis BW, Keating CD.** 2014. Phase separation as a possible means of nuclear compartmentalization. Int. Rev. Cell Mol. Biol. **307:**109-149.
70. **Brangwynne CP, Mitchison TJ, Hyman AA.** 2011. Active liquid-like behavior of nucleoli determines their size and shape in Xenopus laevis oocytes. Proc. Natl. Acad. Sci. U. S. A. **108:**4334-4339.
71. **Louvet E, Yoshida A, Kumeta M, Takeyasu K.** 2014. Probing the stiffness of isolated nucleoli by atomic force microscopy. Histochem. Cell Biol. **141:**365-381.
72. **Freed EF, Prieto JL, McCann KL, McStay B, Baserga SJ.** 2012. NOL11, implicated in the pathogenesis of North American Indian childhood cirrhosis, is required for pre-rRNA transcription and processing. PLoS Genet. **8:**e1002892.

Figure 1

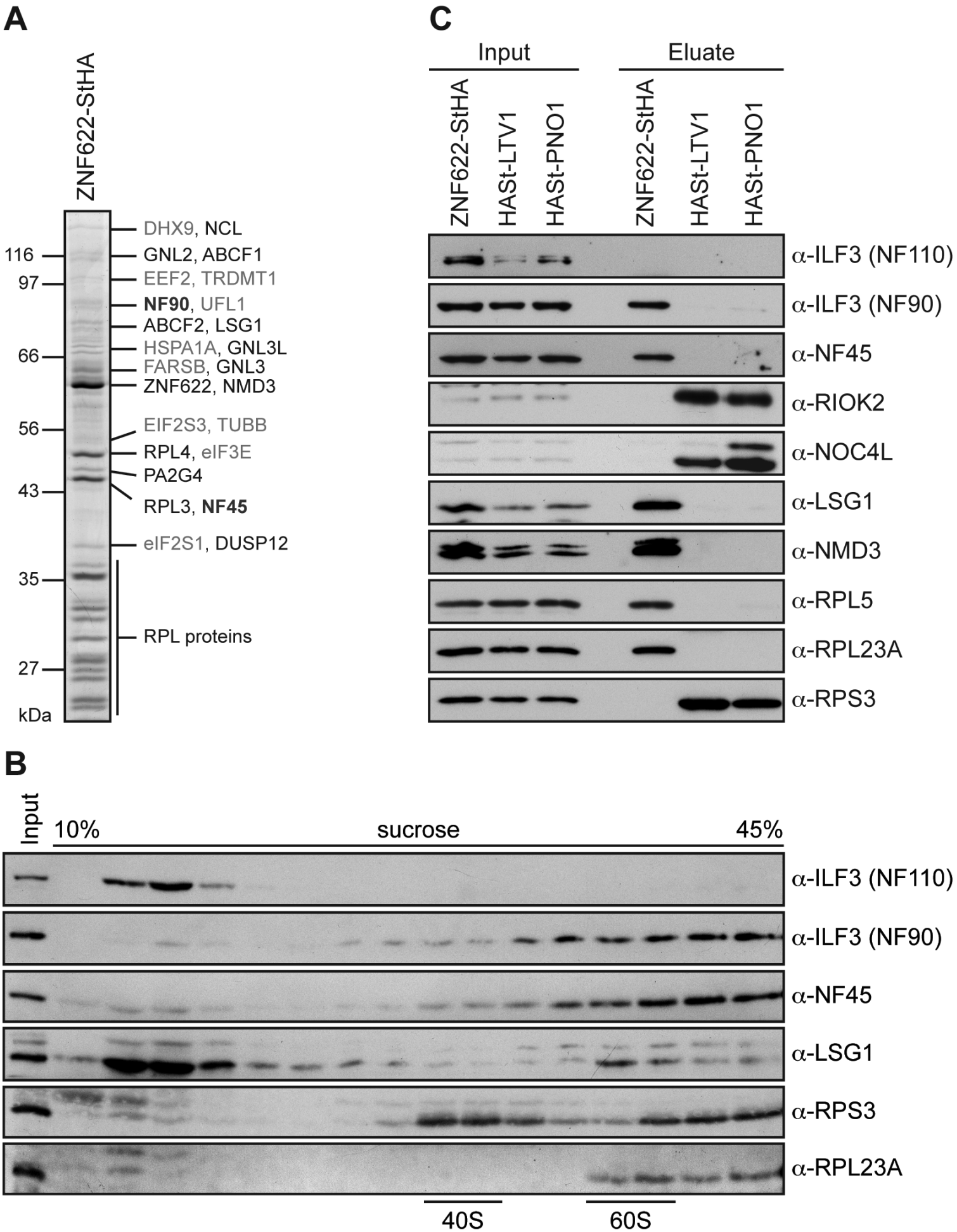
A
ZNF622-StHA
116
97
66
56
43
35
27
kDa
DHX9, NCL
GNL2, ABCF1
EEF2, TRDMT1
NF90, UFL1
ABCF2, LSG1
HSPA1A, GNL3L
FARSB, GNL3
ZNF622, NMD3
EIF2S3, TUBB
RPL4, eIF3E
PA2G4
RPL3, NF45
eIF2S1, DUSP12
RPL proteins
C
Input
Eluate
ZNF622-StHA
HASt-LTV1
HASt-PNO1
ZNF622-StHA
HASt-LTV1
HASt-PNO1
α-ILF3 (NF110)
α-ILF3 (NF90)
α-NF45
α-RIOK2
α-NOC4L
α-LSG1
α-NMD3
α-RPL5
α-RPL23A
α-RPS3
B
Input
10%
sucrose
45%
α-ILF3 (NF110)
α-ILF3 (NF90)
α-NF45
α-LSG1
α-RPS3
α-RPL23A
40S
60S

Figure 2

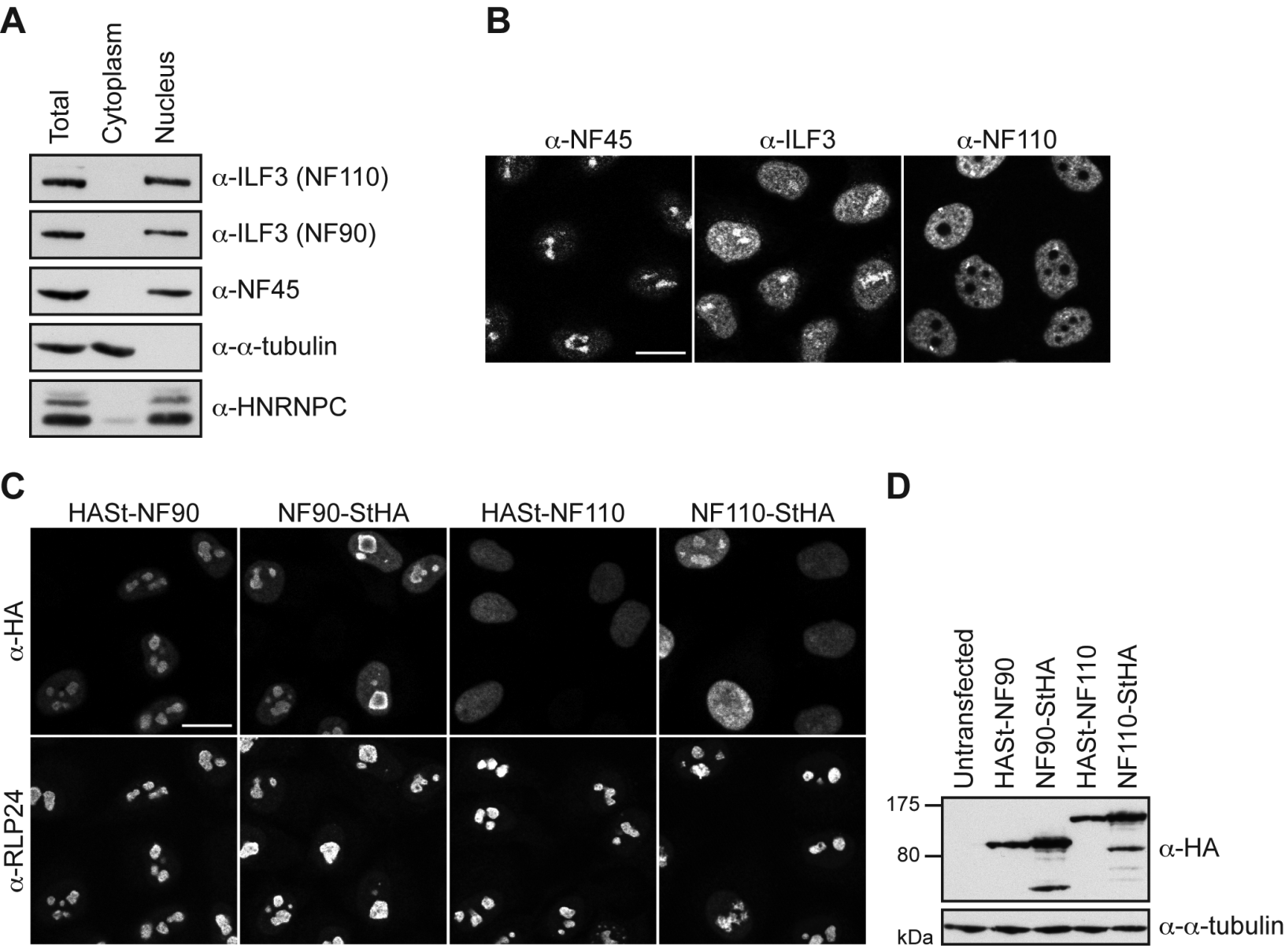
A
Total
Cytoplasm
Nucleus
α-ILF3 (NF110)
α-ILF3 (NF90)
α-NF45
α-α-tubulin
α-HNRNPC
B
α-NF45
α-ILF3
α-NF110
C
HASt-NF90
NF90-StHA
HASt-NF110
NF110-StHA
α-HA
α-RLP24
D
Untransfected
HASt-NF90
NF90-StHA
HASt-NF110
NF110-StHA
175
80
kDa
α-HA
α-α-tubulin

Figure 3

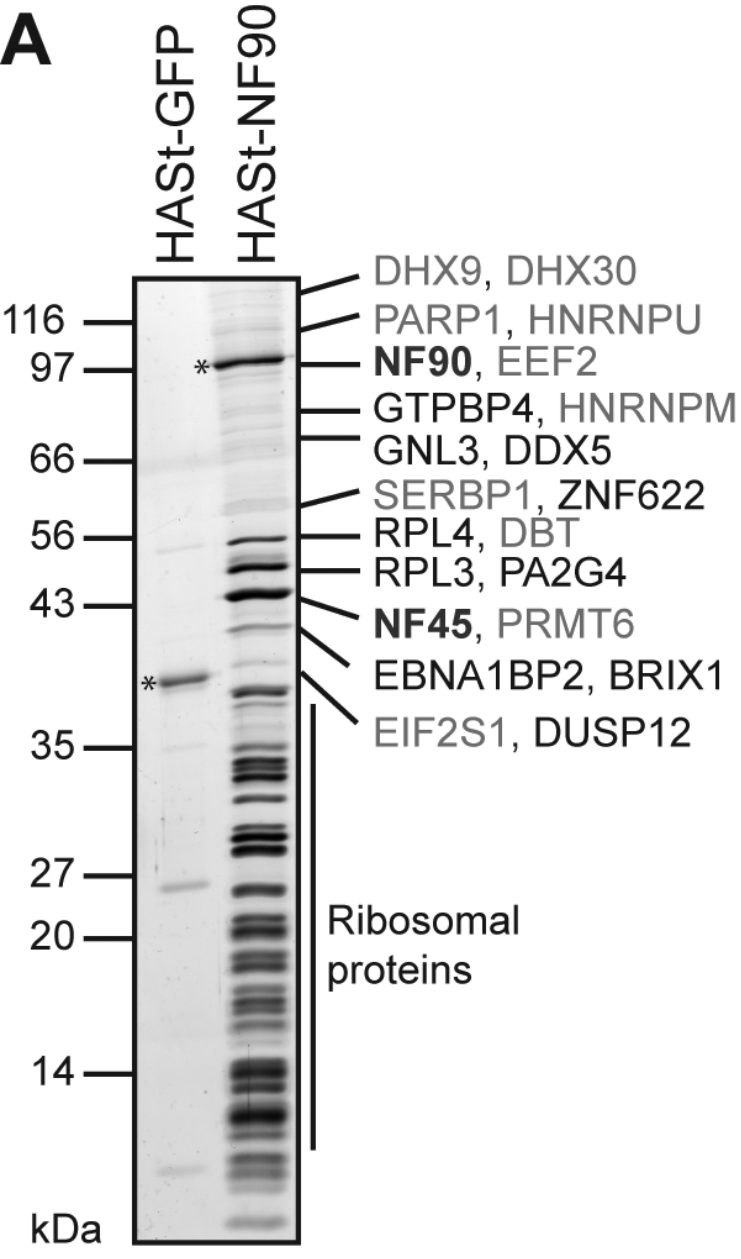
A
HASt-GFP
HASt-NF90
116
97
66
56
43
35
27
20
14
kDa
*
*
DHX9, DHX30
PARP1, HNRNPU
NF90, EEF2
GTPBP4, HNRNPM
GNL3, DDX5
SERBP1, ZNF622
RPL4, DBT
RPL3, PA2G4
NF45, PRMT6
EBNA1BP2, BRIX1
EIF2S1, DUSP12
Ribosomal proteins

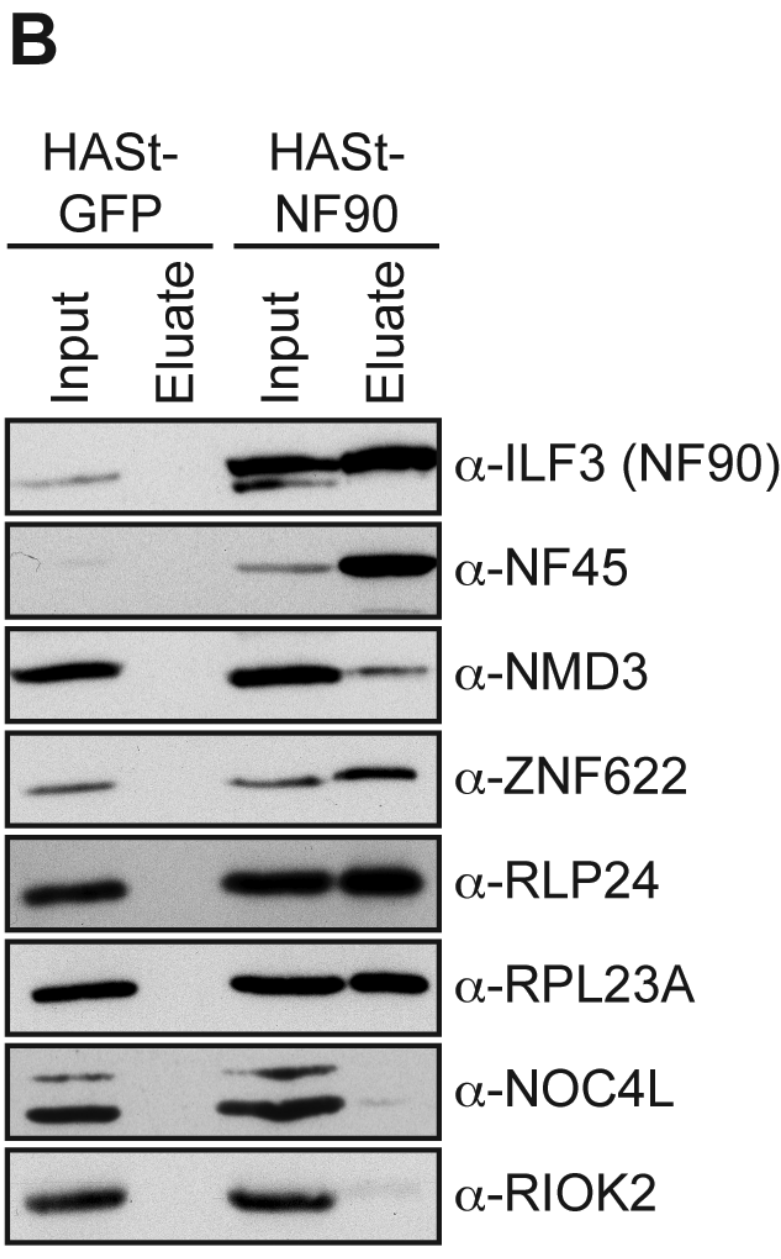
B
HASt-GFP
HASt-NF90
Input
Eluate
Input
Eluate
α-ILF3 (NF90)
α-NF45
α-NMD3
α-ZNF622
α-RLP24
α-RPL23A
α-NOC4L
α-RIOK2

Figure 4

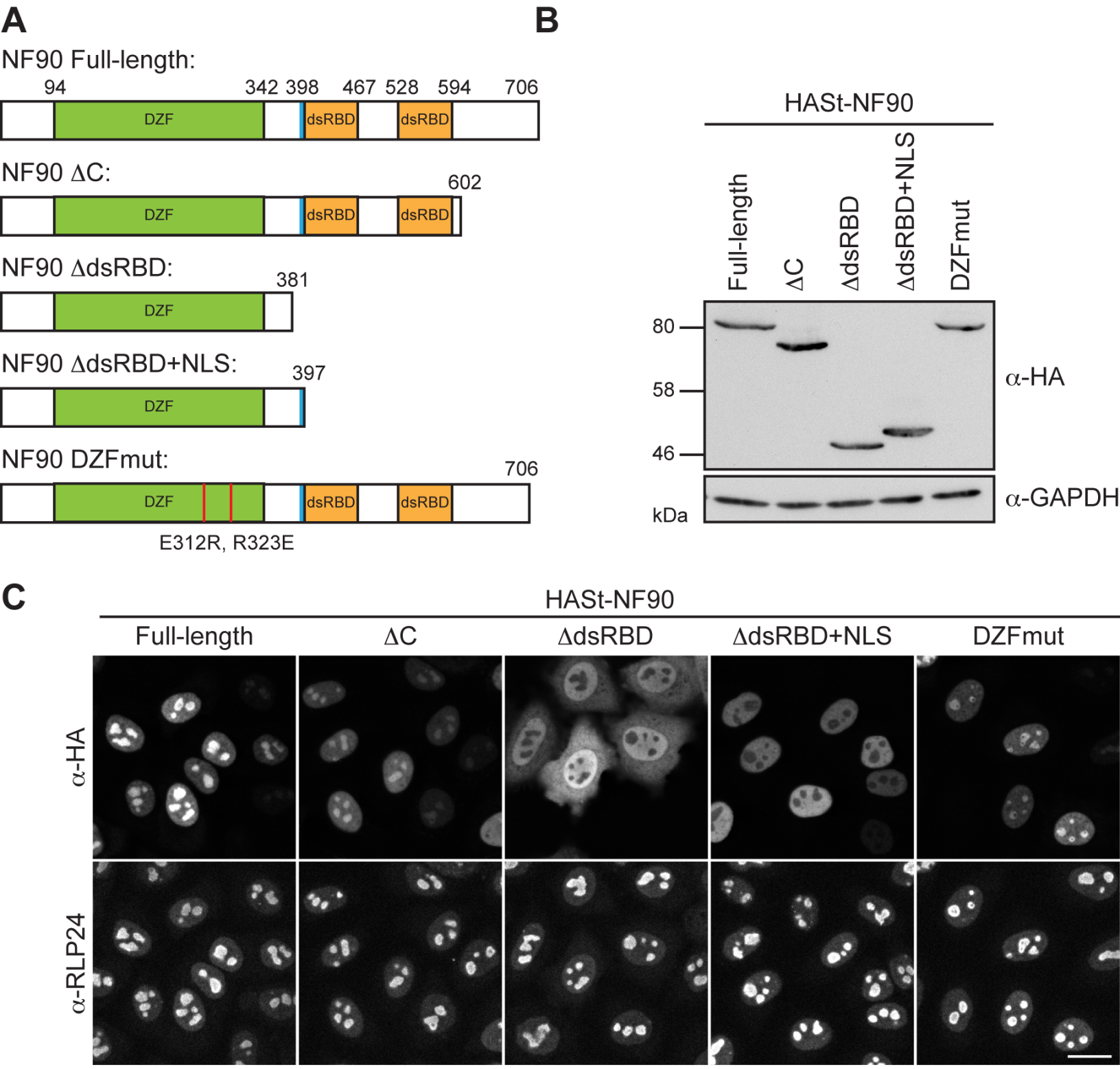
A
NF90 Full-length:
94
342 398
467 528
594
706
DZF
dsRBD
dsRBD
NF90 ΔC:
602
NF90 ΔdsRBD:
381
NF90 ΔdsRBD+NLS:
397
NF90 DZFmut:
706
E312R, R323E
B
HASt-NF90
Full-length
ΔC
ΔdsRBD
ΔdsRBD+NLS
DZFmut
80
58
46
kDa
α-HA
α-GAPDH
C
HASt-NF90
Full-length
ΔC
ΔdsRBD
ΔdsRBD+NLS
DZFmut
α-HA
α-RLP24

Figure 5

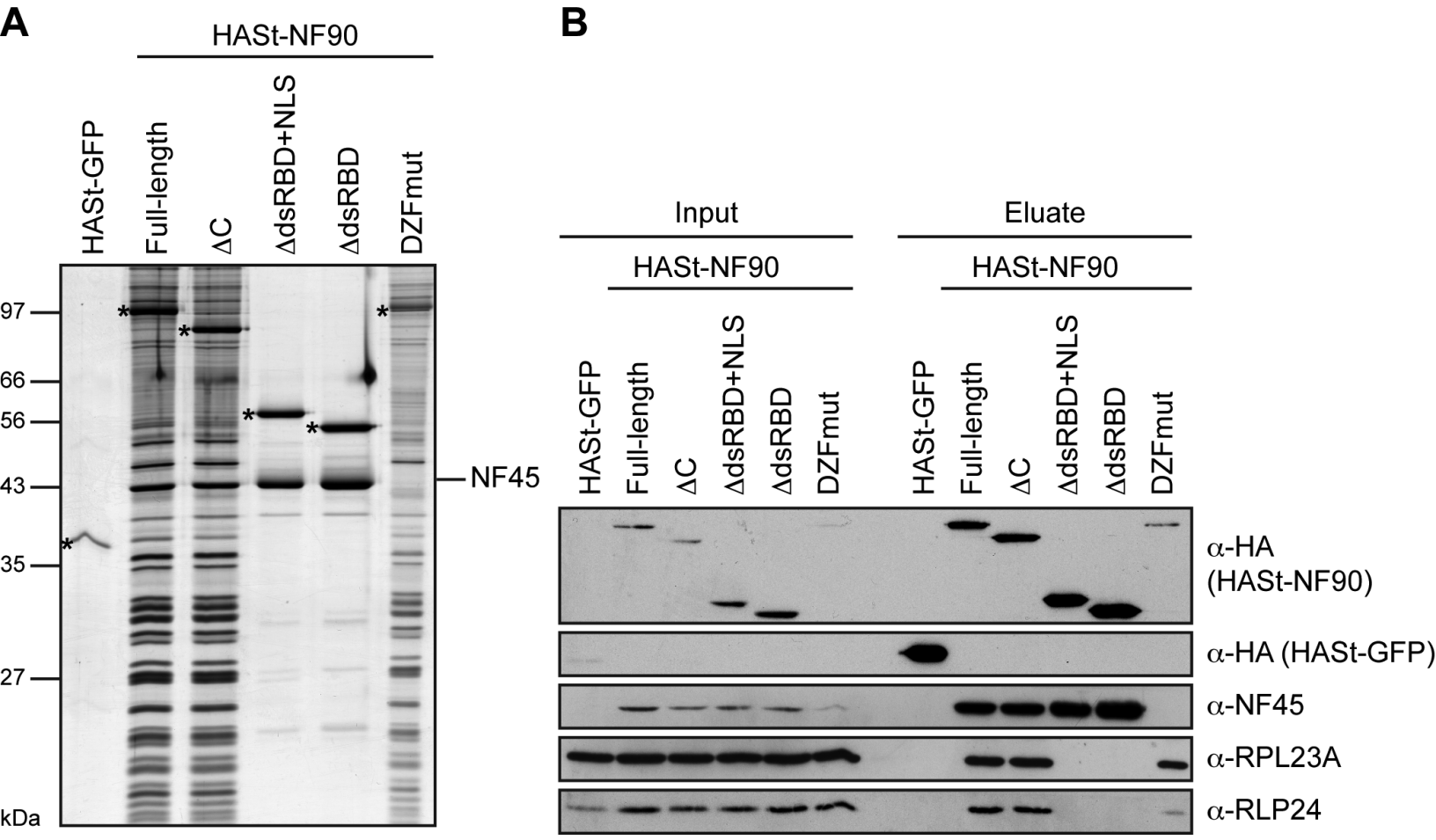
A
HASt-NF90
HASt-GFP
Full-length
ΔC
ΔdsRBD+NLS
ΔdsRBD
DZFmut
97
66
56
43
35
27
kDa
NF45
B
Input
Eluate
HASt-NF90
HASt-NF90
HASt-GFP
Full-length
ΔC
ΔdsRBD+NLS
ΔdsRBD
DZFmut
HASt-GFP
Full-length
ΔC
ΔdsRBD+NLS
ΔdsRBD
DZFmut
α-HA
(HASt-NF90)
α-HA (HASt-GFP)
α-NF45
α-RPL23A
α-RLP24

Figure 6

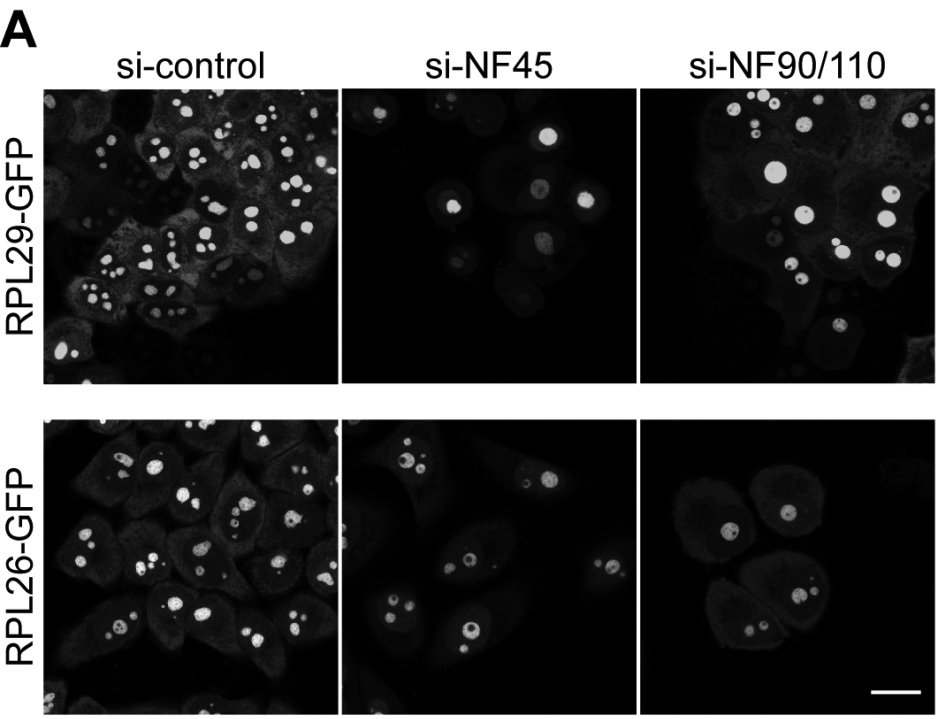
A
si-control
si-NF45
si-NF90/110
RPL29-GFP
RPL26-GFP

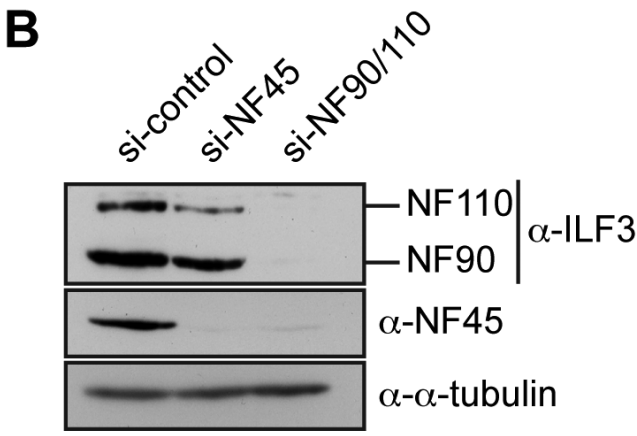
B
si-control
si-NF45
si-NF90/110
NF110
NF90
α-ILF3
α-NF45
α-α-tubulin

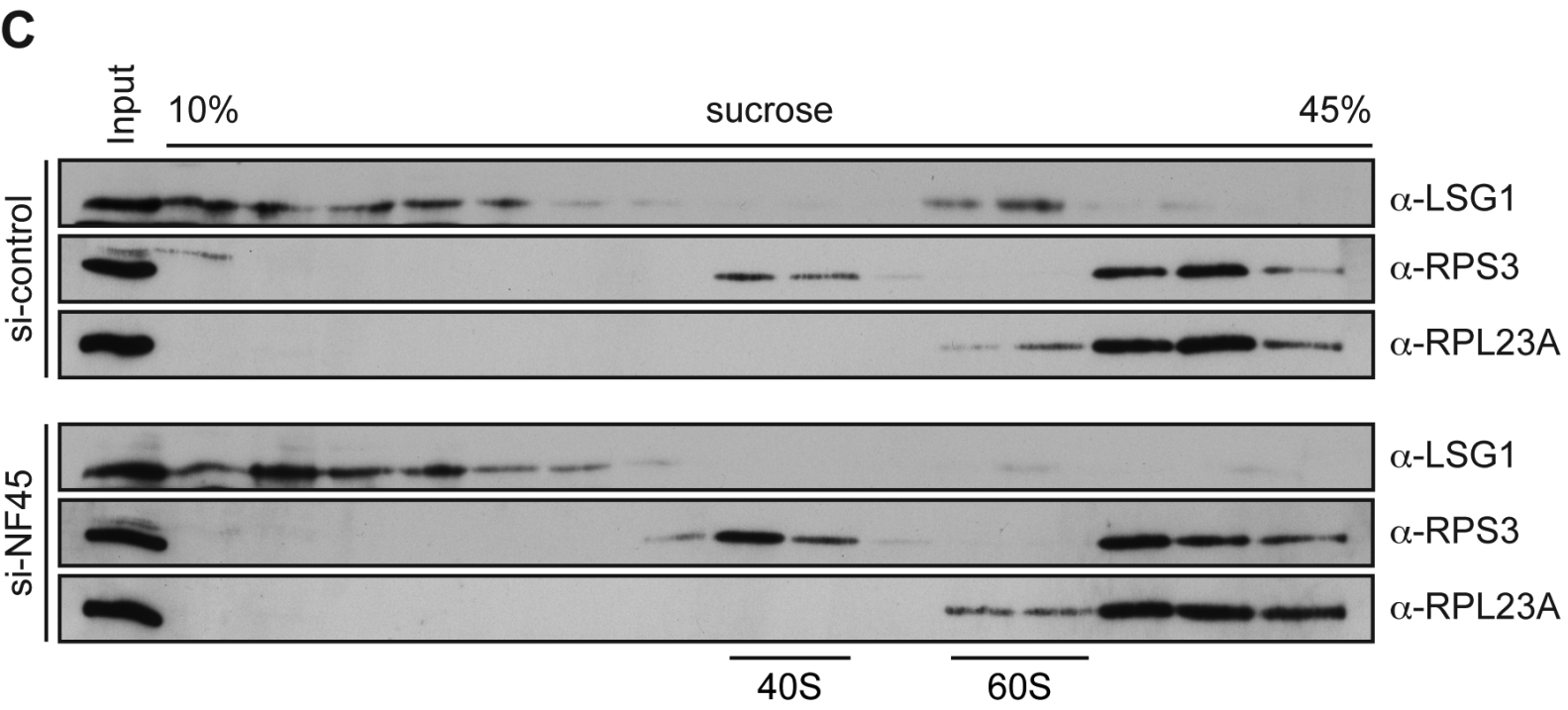
C
Input
10%
sucrose
45%
si-control
si-NF45
α-LSG1
α-RPS3
α-RPL23A
40S
60S

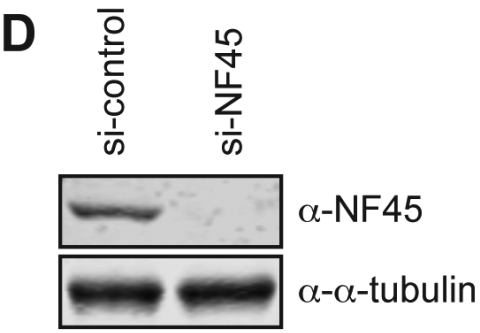
D
si-control
si-NF45
α-NF45
α-α-tubulin

Figure 7

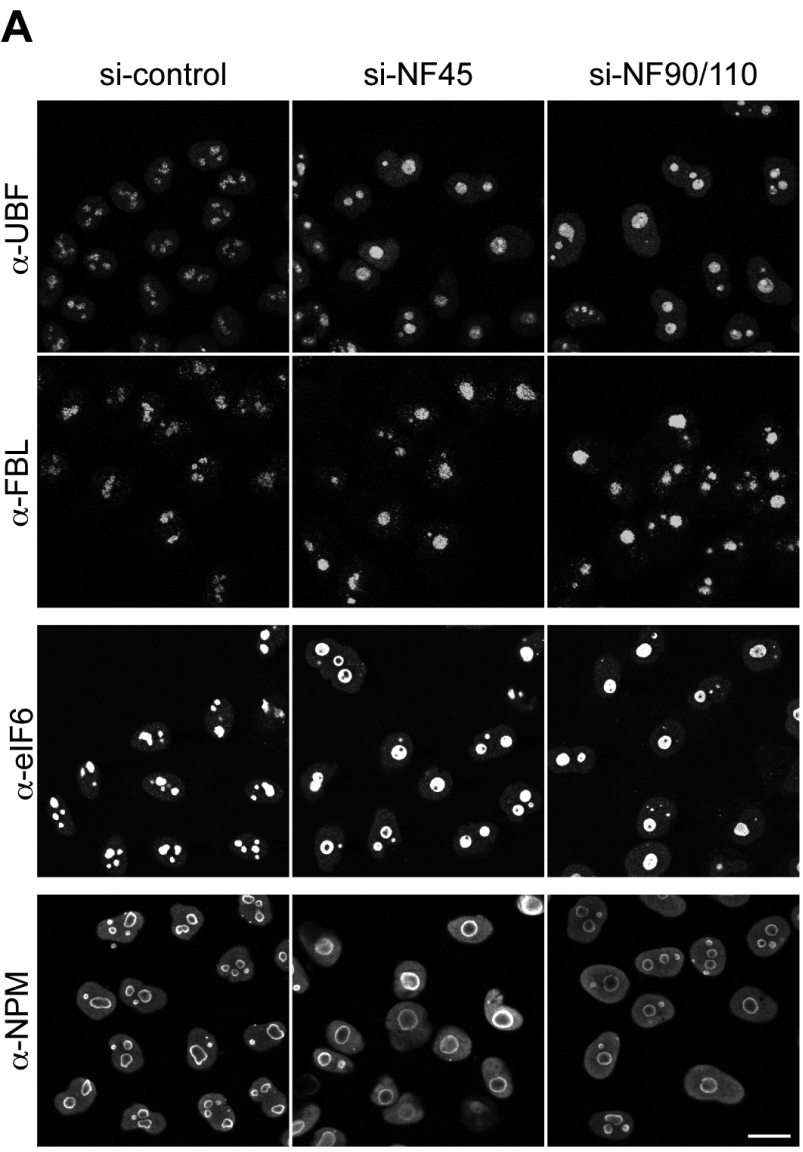
A
si-control
si-NF45
si-NF90/110
α-UBF
α-FBL
α-eIF6
α-NPM

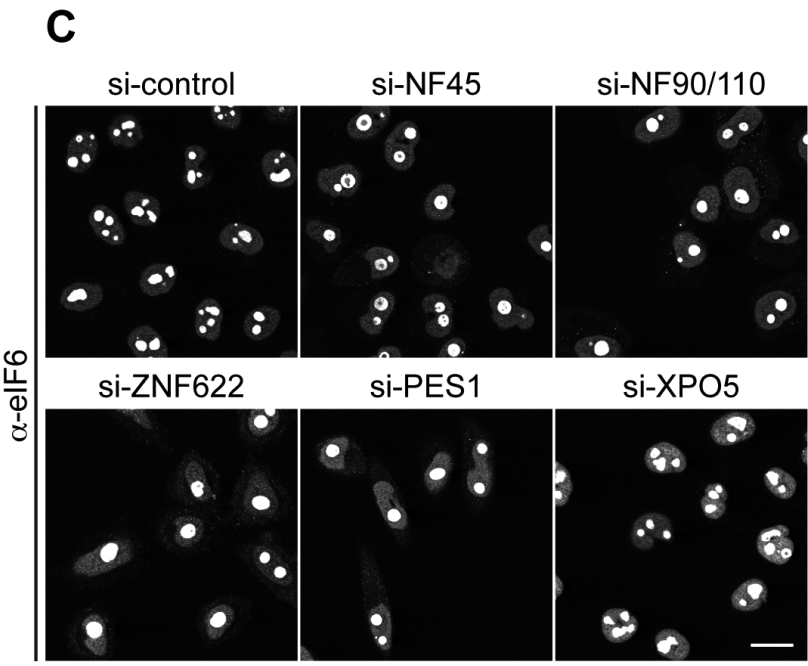
C
si-control
si-NF45
si-NF90/110
si-ZNF622
si-PES1
si-XPO5
α-eIF6

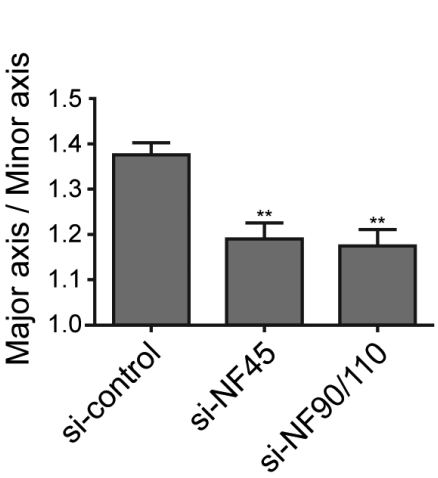
B
Major axis / Minor axis
1.5
1.4
1.3
1.2
1.1
1.0
**
**
si-control
si-NF45
si-NF90/110

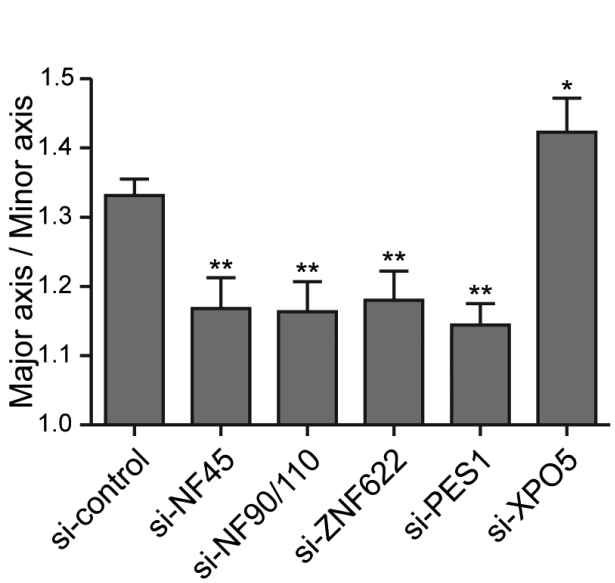
D
Major axis / Minor axis
1.5
1.4
1.3
1.2
1.1
1.0
**
**
**
**
*
si-control
si-NF45
si-NF90/110
si-ZNF622
si-PES1
si-XPO5

Figure 8

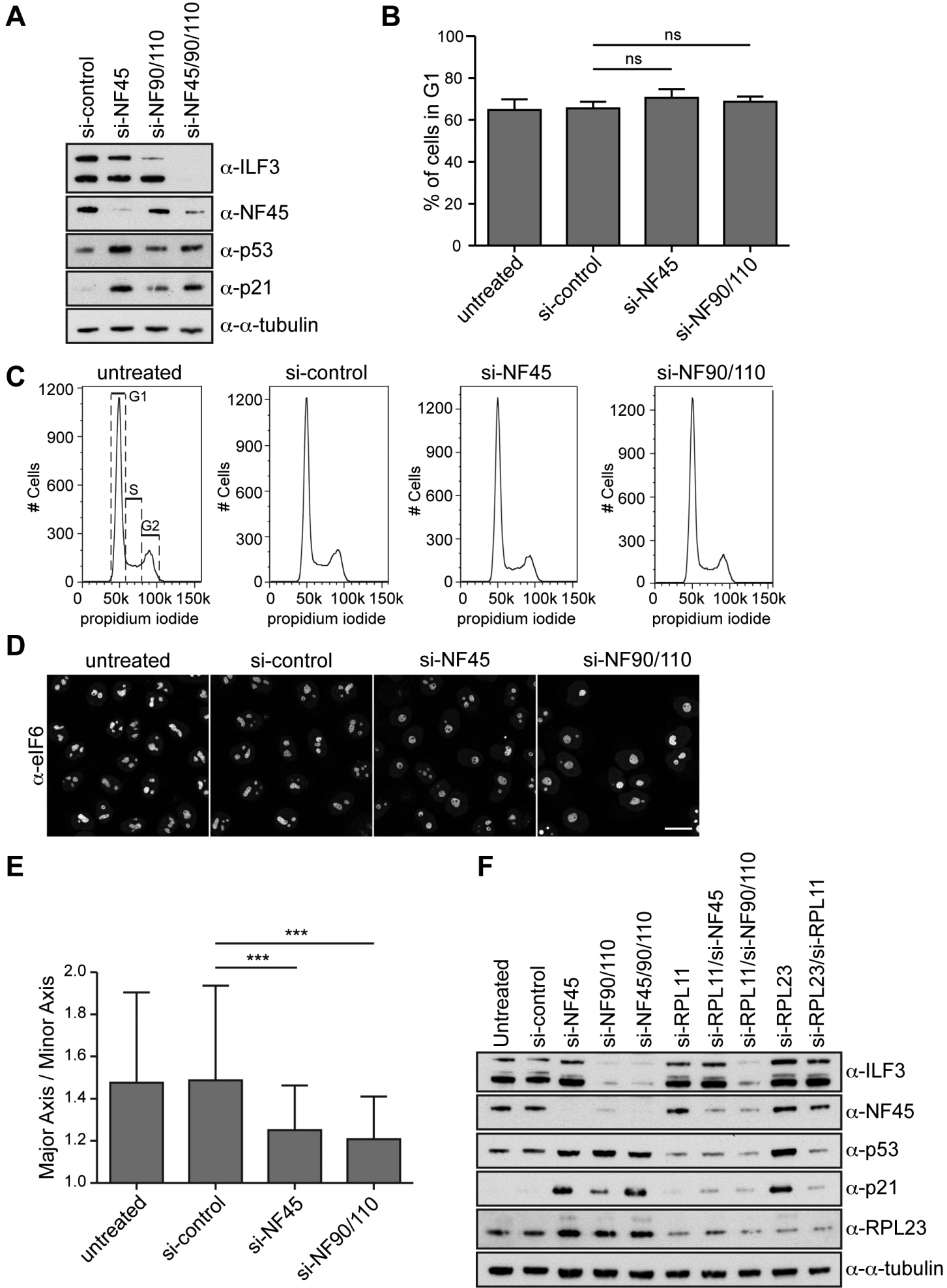
A
si-control
si-NF45
si-NF90/110
si-NF45/90/110
α-ILF3
α-NF45
α-p53
α-p21
α-α-tubulin
B
% of cells in G1
ns
ns
untreated
si-control
si-NF45
si-NF90/110
C
untreated
si-control
si-NF45
si-NF90/110
Cells
G1
S
G2
propidium iodide
D
untreated
si-control
si-NF45
si-NF90/110
α-eIF6
E
Major Axis / Minor Axis
***
***
untreated
si-control
si-NF45
si-NF90/110
F
Untreated
si-control
si-NF45
si-NF90/110
si-NF45/90/110
si-RPL11
si-RPL11/si-NF45
si-RPL11/si-NF90/110
si-RPL23
si-RPL23/si-RPL11
α-ILF3
α-NF45
α-p53
α-p21
α-RPL23
α-α-tubulin